



Published in final edited form as:

*Sci Signal*. ; 14(671): . doi:10.1126/scisignal.abd2639.

## Control of ribosomal protein synthesis by the Microprocessor complex

Xuan Jiang<sup>1, #</sup>, Amit Prabhakar<sup>1</sup>, Stephanie M. Van der Voorn<sup>1, 2</sup>, Prajakta Ghatpande<sup>1</sup>, Barbara Celona<sup>1</sup>, Srivats Venkataramanan<sup>3</sup>, Lorenzo Calviello<sup>3</sup>, Chuwen Lin<sup>1, †</sup>, Wanpeng Wang<sup>1</sup>, Brian L. Black<sup>1, 4</sup>, Stephen N. Floor<sup>3, 5</sup>, Giorgio Lagna<sup>1, 6</sup>, Akiko Hata<sup>1, 4, \*</sup>

<sup>1</sup>Cardiovascular Research Institute, University of California, San Francisco, San Francisco, CA 94143, USA <sup>2</sup>Department of Medical Physiology, University Medical Center Utrecht, Utrecht, 3584 CM, The Netherlands <sup>3</sup>Department of Cell and Tissue Biology, University of California, San Francisco, San Francisco, CA 94143, USA <sup>4</sup>Department of Biochemistry and Biophysics, University of California, San Francisco, CA 94143, USA <sup>5</sup>Helen Diller Family Comprehensive Cancer Center, University of California, San Francisco, San Francisco, California, CA 94143, USA <sup>6</sup>Department of Cellular and Molecular Pharmacology, University of California, San Francisco, San Francisco, CA 94143, USA

### Abstract

Ribosome biogenesis in eukaryotes requires the coordinated production and assembly of 80 ribosomal proteins and 4 ribosomal RNAs (rRNAs), and its rate must be synchronized with cellular growth. Here, we showed that the Microprocessor complex—which mediates the first step of microRNA processing—potentiated the transcription of ribosomal protein genes by eliminating DNA/RNA hybrids known as R-loops. Nutrient deprivation triggered the nuclear export of Droscha, a key component of the Microprocessor complex, and its subsequent degradation by the E3 ubiquitin ligase Nedd4, thereby reducing ribosomal protein production and protein synthesis. In mouse erythroid progenitors, conditional deletion of *Droscha* led to the reduced production of ribosomal proteins, translational inhibition of the mRNA encoding the erythroid transcription factor Gata1, and impaired erythropoiesis. This phenotype mirrored the clinical presentation of human “ribosomopathies”. Thus, the Microprocessor complex plays a pivotal role in

\* **Correspondence Author:** Akiko Hata, PhD, Mail Code: 3118, 555 Mission Bay Blvd. South, SCVRB, Room 252T, San Francisco, CA 94143, USA. Tel. 415-476-9758; Fax: 415-514-1173, akiko.hata@ucsf.edu.

# **Present Address:** Department of Immunology, Zhongshan School of Medicine, Sun Yat-sen University, Guangzhou 510089, P.R. China

† **Present Address:** Department of Histology and Embryology, Zhongshan School of Medicine, Sun Yat-sen University, Guangzhou 510089, P.R. China

Author Contributions

J.X., A.P., S. VDV, P.G., L.C., B.C., C.L., W.W. and S.V. designed the experiments and conducted the experiments. B.L.B., S.N.F., G.L. and A.H. designed the experiments and wrote the paper. All authors reviewed and approved the manuscript.

Competing Interests

The authors declare that they have no competing interests except S.N.F. consults for MOMA Therapeutics.

Data and Materials availability

RNA sequencing data are available at the NCBI Sequence Read Archive (SRA): GEO Accession Number GSE160832. Proteomics data are found in Data File S1 and the raw data are available at the Integrated Proteome Resources (iProX): project ID: IPX0002684000. All other data needed to evaluate the conclusions in the paper are present in the paper or the Supplementary Materials.

synchronizing protein synthesis capacity with cellular growth rate and is a potential drug target for anemias caused by ribosomal insufficiency.

---

## Introduction

Regulation of protein synthesis is essential to cell growth, differentiation, and homeostasis, and hinges on the ribosome, the protein synthesis apparatus composed of 80 ribosomal proteins (RPs) and 4 ribosomal RNAs (rRNAs) in eukaryotes. Because ribosomes are abundant, it is crucial that the synthesis of RPs is coordinated with that of rRNAs and is synchronized with cell growth rate. Insufficient ribosome numbers and mutations in RPs underlie human diseases known as ribosomopathies, which include Diamond-Blackfan anemia (DBA), 5q-myelodysplastic syndrome, and T cell acute lymphoblastic leukemia. In DBA patients, ribosome insufficiency impairs translation of *Gata1*—a transcription factor essential for erythropoiesis—and causes anemia(1).

Because ribosome biogenesis is an energy-intensive process, cells conserve energy by coordinating the synthesis of RPs and rRNAs with the demand for protein synthesis as determined by the cellular environment (2). In *E. coli*, 54 RP genes (RPGs) are encoded in 20 operons and regulated by a translational feedback mechanism in which specific RPs directly bind to their own mRNAs and inhibit translation (3, 4). In eukaryotes, RPGs are regulated at different steps of their synthesis, including RPG transcription, mRNA splicing and translation (5, 6). In yeast, RPGs are largely regulated by transcription factors, such as Ifh1, Fhl1, and Rap1 (7–12), which enable synchronized RP biosynthesis. A small number of yeast RPs, such as Rpl33p, Rps14p, and Rpl22p, bind to their own precursor-mRNAs (pre-mRNA) and inhibit splicing to provide negative feedback regulation (13, 14). In multicellular organisms, all RPGs contain a sequence of 5–15 pyrimidines known as “the 5′ terminal oligopyrimidine (5′ TOP) motif” at the TSS, which has been proposed to play a role in coordinating RP synthesis (15–17). Different molecules have been identified to associate with some of the TOP sequences in both DNA and RNA, including DNA-binding proteins [zinc finger protein 9 (ZFP9)](18–20), RNA-binding proteins [T cell intracellular antigen-1 (TIA-1), TIA-1-related (TIAR) (21), and La-related protein 1 (LARP1) (22–27) and microRNA-10a (28), but a factor that can control the expression of all RPGs through the 5′ TOP motif remains to be found. We propose that the Microprocessor might play this role.

The Microprocessor complex comprises two core components, the ribonuclease (RNase) III Drosha and its cofactor Dgcr8. It is essential for the biogenesis of most microRNAs (miRNAs), short RNAs that repress gene expression by binding to mRNAs and targeting them for degradation and/or preventing their translation (29). The Microprocessor localizes predominantly in the nucleus, where it recognizes a hairpin structure in the primary-miRNA (pri-miRNA) transcript and cleaves its 5′ and 3′ flanking single-stranded RNA (ssRNA) to generate the stem-loop precursor-miRNA (pre-miRNA). The pre-miRNA is the substrate for Dicer processing in the cytoplasm. The processing of pri-miRNA by the Microprocessor is regulated by multiple accessory proteins that are components of the larger Microprocessor complex, including the DEAD-box RNA helicase 5 (Ddx5) and Ddx17 (30). In addition to miRNA biogenesis, the Microprocessor complex has various miRNA-independent functions,

including (i) cleavage of a hairpin structure in selected mRNAs and their destabilization (31, 32), (ii) processing of rRNAs (33), (iii) regulation of RNAPII-mediated transcription (34), (iv) maintenance of genome integrity by facilitating DNA damage responses (35–37), and (v) antiviral defense by cleavage of viral RNAs (38, 39). Although the RNase activity of the Microprocessor is well documented, a role for the RNA helicases (such as Ddx5 and Ddx17) in pri-miRNA processing or in the miRNA-independent functions of the Microprocessor remains unknown. We propose that the Microprocessor-associated RNA helicase Ddx5 plays a key role in resolving R-loops.

A three-stranded nucleic acid structure known as an R-loop transiently forms during transcription (40). It is composed of a DNA/RNA hybrid (a single-stranded template DNA (ssDNA) hybridized with a nascent mRNA) and an associated non-template ssDNA(40). Extended or persistent formation of R-loops during transcription can affect the activity of RNA polymerase (RNAP) and alter gene expression (40). The abundance of R-loops is determined by the balance between the formation and resolution of DNA/RNA hybrids. Various factors have been implicated in the control of R-loop homeostasis, including transcription factors, helicases, ribonucleases, topoisomerases, chromatin remodelers, and proteins involved in DNA repair and RNA surveillance (40). Deregulation of R-loops, which results in aberrant gene expression and chromatin structure, increases DNA breaks and genome instability, contributing to neurological disorders and tumorigenesis (40).

Here we report that the Microprocessor complex associated with RPG loci, removed R-loops, and facilitated transcription elongation. This process required the helicase activity of Ddx5 but not the ribonuclease activity of the Microprocessor or miRNA biogenesis. Nutrient depletion reduced Drosha protein and inhibited RP synthesis; conversely, exogenous expression of Drosha prevented the inhibition of RP synthesis by nutrient depletion. Mice lacking *Drosha* showed impaired erythropoiesis and anemia due to reduced *Gata1* translation by insufficient ribosome numbers, a mechanism consistent with human ribosomopathies, thus demonstrating the physiological importance of this new function of the Microprocessor complex.

## Results

### Endothelial-specific deletion of *Drosha* in mice impairs erythropoiesis

Mice with an endothelial-specific deletion of *Drosha* (hereafter referred to as *Drosha*-cKO mice) die around embryonic day (E)14.5–15.5 due to an erythropoiesis defect (41). Although the number of erythroid progenitor cells (EPCs) was similar in *Drosha*-cKO and control mice (littermates with at least one wild-type *Drosha* allele, hereafter referred to as Ctrl) in the yolk sac (YS) at E9.5 (Fig. 1a), their ability to differentiate into mature erythroid cells as measured by a methylcellulose colony-forming unit (CFU) assay was severely affected by deletion of *Drosha* (Fig. 1b). To measure the effect of *Drosha* on erythroid differentiation in vivo, we separated EPCs from the peripheral blood of E10.5 *Drosha*-cKO and Ctrl embryos according to their differentiation stage, more mature erythroid precursors (MEPs, CD71<sup>high</sup>Ter119<sup>high</sup>) and immature erythroid precursors (IEPs, CD71<sup>high</sup>Ter119<sup>low</sup>) (42). The percentage of IEPs rose from 1% in Ctrl embryos to 12.5% in cKO embryos (Fig. 1c), whereas MEPs decreased from 30% to 19% (Fig. 1c). Further analysis showed that the

residual MEPs in cKO embryos retained at least one intact *Drosha* allele and expressed *Drosha* mRNA at a level comparable to that in MEPs in Ctrl embryos (Supplementary Fig. S1a). This finding confirmed that the presence of Drosha was critical for EPC maturation. In older embryos (E13.5), IEPs remained predominant in *Drosha* cKO (Fig. 1d: 29.1% cKO compared to 7.3% Ctrl) at the expense of MEPs (Fig. 1d: 15.4% cKO compared to 80.6% Ctrl). When cultured in erythrocyte differentiation media for 3 days, >95% of cKO IEPs remained morphologically immature, whereas ~25% of Ctrl IEPs developed a mature erythrocyte morphology (Supplementary Fig. S1b). These results suggest that in the absence of Drosha, EPCs fail to differentiate into erythrocytes.

To elucidate the molecular mechanism underlying the maturation defects of EPCs in *Drosha* cKO embryos, we analyzed in IEPs (CD71<sup>high</sup>Ter119<sup>low</sup>) the expression of mRNAs encoding transcription factors involved in erythroid differentiation, such as *Gata binding protein 1 (Gata1)* (43, 44), *Friend of Gata1 (Fog1)*, also known as *ZFPM1*, *T cell acute lymphocytic leukemia 1 (TAL1)*, also known as *SCL*, and *Krüppel-like factor 1 (KLF1)*, also known as *EKLF*. The mRNAs encoding these transcription factors were expressed at comparable levels in cKO and Ctrl embryos, although *Drosha* mRNA was 70% lower in cKO embryos than in Ctrl embryos, as expected (Fig. 1e.) However, Gata1 protein, which was abundant in Ctrl embryos, was undetectable in cKO embryos (Fig. 1f). Furthermore, transcripts for Gata1 target genes—such as *Alas2*, *Hbb-a*, *Hbb-b*, and *Epb4.9* (45)—were reduced in cKO embryos compared to Ctrl embryos (Fig. 1e), consistent with the loss of Gata1 protein. We observed a similar reduction in Gata1 protein (Fig. 1f, **left**), but not in *Gata1* mRNA (Fig. 1f, **right**), in human erythroleukemia K562 cells in which the *Drosha* gene was mutated by CRISPR/Cas9 (*Drosha* KO cells). Loss of Gata1 protein in *Drosha* KO cells was not reversed by the proteasome inhibitor MG132 (Fig. 1g), suggesting that a mechanism other than protein degradation was responsible for the reduction in Gata1 abundance. Cell growth analysis showed that *Drosha* KO cells grew at a ~50% lower rate than Ctrl K562 cells but appeared otherwise normal (Supplementary Fig. S2a). The microRNA-451 (miR-451), which is critical for erythroid differentiation(46), was abundant in *Drosha* KO cells (Supplementary Fig. S2b). K562 cells undergo partial differentiation into benzidine-positive (and therefore blue) mature erythrocytes when treated with hemin, a ferric (Fe<sup>3+</sup>) form of heme(47). Whereas ~60% Ctrl K562 cells turned benzidine-positive, *Drosha* KO cells treated with hemin remained benzidine-negative and undifferentiated (Supplementary Fig. S2c), confirming a requirement of Drosha for erythrocyte differentiation, as seen in cKO mice (Fig. 1c and 1d). Furthermore, polysome fractionation analysis showed that in Ctrl K562 cells, *Gata1* mRNA was enriched in the high molecular weight polysome fractions, an indicator of active translation (Fig. 1h, **bottom, black line**). In *Drosha* KO cells, however, *Gata1* mRNA (Fig. 1h, **bottom, red line**) was enriched in monosome fractions overlapping with *ATF4* mRNA (Fig. 1h, **bottom, orange and blue lines**), which is translationally inhibited and inactivated in cells under regular growth conditions. Thus, we conclude that depletion of Drosha in erythroid progenitors results in decreased *Gata1* translation, which curtails erythroid maturation.

## The Microprocessor regulates RPGs

To elucidate the molecular mechanism underlying the attenuation of *Gata1* translation upon depletion of Droscha, we performed RNA-seq analysis on EPCs. As expected, the amount of *Droscha* mRNA was reduced in cKO EPCs compared to Ctrl EPCs (Fig. 2a). Depletion of Droscha in cKO EPCs was also validated by an increase in the abundance of transcripts processed and degraded by Droscha, such as *Dgcr8*, *Anks6*, and *Stat6* (31) (Supplementary Fig. S3a). ~60% of transcripts were increased in cKO EPCs compared to Ctrl EPCs, likely reflecting a global reduction of miRNAs and derepression of their mRNA targets. Kyoto Encyclopedia of Genes and Genomes (KEGG) pathway analysis revealed that genes annotated with “ribosome” were overrepresented among genes that were decreased in cKO EPCs compared to Ctrl EPCs (Fig. 2b). Similarly, Gene Ontology analysis of cellular components and biological processes both showed an overrepresentation of genes associated with “ribosome”, “ribosome biogenesis”, and “translation” among the genes reduced in cKO EPCs (Supplementary Fig. S3b). Of 71 small (40S) ribosomal protein (Rps) and large (60S) ribosomal protein (Rpl)-encoding transcripts, 68 (96%) were decreased on average by 25% in cKO EPCs (Fig. 2a), a result confirmed by qRT-PCR analysis (Fig. 2c and Supplementary Fig. S3c).

Similar to primary mouse EPCs, *Rps* and *Rpl* mRNAs also decreased in K562 cells with *Droscha* silencing (Fig. 2a). Tandem mass-tag-based quantitative proteomic analysis (Fig. 2d, Supplementary Fig. S4 and Data File S1) indicated that the majority of Rps and Rpl proteins decreased in *Droscha*-depleted K562 cells (Fig. 2d and Supplementary Fig. S4), a finding confirmed by immunoblot analyses (Fig. 2e). To examine how the rate of global protein synthesis was affected due to reduced RP abundance in *Droscha*-null cells, we performed a puromycin incorporation assay (also known as puromycin-associated nascent chain proteomics; PUNCH-P)(48). Puromycin is an analog of tyrosyl-tRNA that is incorporated into nascent polypeptide chains, allowing the measurement of global protein synthesis through the detection of puromycin-labeled proteins with a puromycin antibody (48). Equal numbers of EPCs were sorted from the peripheral blood of E11.5 Ctrl or cKO embryos from puromycin-injected pregnant mice. The amount of puromycin-labeled protein was 90% lower in cKO EPCs compared to Ctrl EPCs (Fig. 2f, **lane 1 compared to 2**), indicating reduced protein synthesis in cKO EPCs. Thus, we conclude that Droscha depletion causes a decrease in RPs and reduction of protein synthesis. The degree of the effect of ribosome insufficiency on translation is mRNA-dependent, and *Gata1* translation appears to be more severely attenuated than that of other housekeeping gene transcripts in EPCs and K562 cells(1). A search of published RNA-seq data revealed that Rps and Rpl mRNAs are also decreased in non-erythroid cells, such as hepatocarcinoma HepG2 and colon carcinoma HCT116 cells (Fig. 2g), upon RNAi-mediated silencing of *Droscha* (49), indicating that the Droscha-RPGs regulatory axis is not confined to erythroid lineages.

We next tested the involvement of other subunits of the Microprocessor complex in the regulation of RPGs. We observed that both DGCR8 (a key partner of Droscha) and the DEAD-box RNA helicase Ddx5 (an auxiliary subunit of the Microprocessor complex) are required for RPG regulation, because nearly all Rps and Rpl mRNAs were reduced in the hearts of E9.5 homozygous *Dgcr8* cKO mice (*Dgcr8*<sup>doxP/loxP</sup>; *Mesp1*<sup>Cre/+</sup>)(50) and in Ddx5-

depleted HepG2 cells (Fig. 2g). However, depletion of Argonaute2 (Ago2), a component of the RNA silencing complex (RISC) that uses miRNAs to inhibit mRNA expression, resulted in a small increase rather than decrease in Rps and Rpl mRNAs in K562 cells (Fig. 2g)(51). If impairment of miRNA synthesis and function were responsible for the RP synthesis block, we would have expected a similar result from depletion of Microprocessor and RISC components. However, this result suggests that miRNA biogenesis may not be the main mechanism driving the regulation of RPGs by the Drosha. To investigate further the possibility of miRNA-independent control of RPGs by the Microprocessor complex, we expressed in HCT116 cells a ribonuclease-defective Drosha mutant (QAQ; R<sup>938</sup>K<sup>939</sup>K<sup>940</sup> to QAQ), which cannot process pri-miRNAs(52). Rps and Rpl mRNAs were increased as effectively by the Drosha QAQ mutant as by WT Drosha when expressed at similar mRNA (Fig. 2h, **top**) and protein (Fig. 2h, **bottom**) levels. In contrast, miR-21 abundance was increased by Drosha WT but not by Drosha QAQ mutant (Fig. 2h). These results confirm that miRNA processing by the Microprocessor complex is dispensable in the regulation of RP expression.

### The Microprocessor complex associates with RPG transcripts

Drosha and Dgcr8 associates with the proximal promoter regions of several genes indirectly through RNAPII (34). Chromatin immunoprecipitation-DNA sequencing (ChIP-seq) analysis indicated that both Drosha and Dgcr8 interact with the genomic loci proximal to the transcription start site (TSS) of all 80 RPGs (Supplementary Fig. S5 and Table 1) (53). The Drosha and Dgcr8 association sites within the *Rps15a*, *Rps24*, *Rpl4*, and *Rpl28* loci overlap with the RNAPII binding sites and is marked by histone H3 Lysine (K) 4 trimethylation (H3K4me3), which indicates transcriptionally active chromatin (Fig. 3a)(53, 54). We validated the association of Drosha with RPG loci by ChIP-qPCR assay in MEFs (Fig. 3b). Transcription inhibition by Actinomycin D (ActD) abolished the association of Drosha with RPG loci (Fig. 3c), as did RNA digestion with ribonuclease A (RNase A), which cleaves single-stranded mRNA (Fig. 3d), indicating the involvement of mRNA in the interaction between Drosha and RPGs. Furthermore, enhanced UV crosslinking followed by immunoprecipitation (eCLIP) performed in K562 cells by ENCODE confirmed that Drosha and Dgcr8, but not polypyrimidine tract binding protein 1 (PTBP1), associates with Rps and Rpl mRNAs (Supplementary Fig. S6) (55). When ChIP samples were pretreated with ribonuclease H (RNase H), which specifically degrades the RNA in a DNA/RNA hybrid, Drosha association with RPG loci was abolished, suggesting that Drosha interacts with the nascent RPG transcript on or near R-loops, which are composed of a DNA/RNA hybrid of template DNA and nascent mRNA and a single-stranded non-template DNA (Fig. 3e). Dgcr8 is not essential for the association of Drosha with RPG loci because Drosha enrichment was similar in *Dgcr8* homozygous-null MEFs compared to WT control MEFs (Fig. 3f). However, the amounts of RPG mRNAs were reduced in *Dgcr8* KO cells (Fig. 3g), suggesting that Dgcr8 is required for transcriptional regulation of RPGs at a stage that follows the binding of Drosha to RPG loci.

### The Microprocessor complex associates with the 5'-TOP motif

A metagene analysis of Drosha eCLIP datasets(55) indicated that Drosha binding is enriched toward the 5'-end of the RPG transcripts (Fig. 4a, **blue line**), whereas Drosha binding to the

non-RPG transcripts is distributed evenly throughout the transcripts (Fig. 4a, **red line**). Because all RPG transcripts in metazoa contain an oligopyrimidine sequence at the 5'-end (5'-TOP motif) that regulates the expression of RPGs (15, 56–58), we speculated that the 5'-TOP motif might play a role in the association of Drosha with the 5'-end of the RPG transcripts. An RNA secondary structure prediction algorithm (Vienna RNAfold) detected a stable stem-loop structure in the first 37-nt sequence of the *Rpl28* mRNA (Fig. 4b, **top**). Electrophoretic mobility shift assays (EMSAs) confirmed that the double-strand RNA binding domain (RBD; amino acids 1259–1337) of Drosha was sufficient to bind the 37–40-nt sequence of the *Rpl28* gene, but failed to bind to the mutant probe, in which three nucleotides within the TOP motif were mutated from UUU to AAA to disrupt both the TOP motif and the stem structure (Fig. 4b, **bottom**), indicating that Drosha could associate with the RPG mRNAs through the TOP motif. To examine the function of the association of Drosha with the 5'-end of RPG mRNAs, a luciferase reporter construct containing the TATA box and the TOP motif of the *Rpl28* gene was transfected into HCT116 cells. Both the reporter activity and the amount of luciferase mRNA were lower in HCT116 cells in which *Drosha* had been deleted by CRISPR/Cas9 compared to control cells, indicating that the WT luciferase reporter recapitulates the Drosha-dependent transcriptional regulation of *Rpl28* (Fig. 4c). The Up-Luc construct (in which the nucleotides upstream of the TSS were mutated) displayed similar reporter activity and mRNA level to the WT luciferase reporter (Fig. 4c). Conversely, a luciferase reporter in which the TOP motif was mutated to abolish binding to the Drosha RBD (Mut-luc) as detected by EMSAs (Fig. 4b), exhibited reduced Luc activity and *Luc* mRNA level and failed to respond to Drosha depletion (Fig. 4c). These results indicate that Drosha specifically associates with the TOP motif, which is common to all RPG mRNAs.

### The helicase Ddx5 reduces R-loops and facilitates transcription elongation

Stable formation of an R-loop, which is composed of the template DNA/nascent mRNA hybrid and the displaced non-template DNA strand, inhibits elongation by RNAPII(40). Genome-wide mapping of R-loops by DNA/RNA immunoprecipitation (DRIP) and sequencing (DRIP-seq) using the S9.6 antibody, which specifically recognizes DNA/RNA hybrids, detected the formation of R-loops at 52 out of 83 RPG loci in human U-2OS cells (Supplementary Fig. S7)(35). Upon *Drosha* depletion, R-loops increased at RPG loci, but not at non-RPG control loci (*GAPDH* and *Tuba1a*) (Fig. 5a)(59). Similar results were obtained by DRIP assay in K562 cells (Fig. 5b, **Ctrl compared to KO**). The DRIP signal was abolished when DNA/RNA hybrids were degraded by RNase H, confirming a specific recognition of DNA/RNA hybrids by the S9.6 antibody (Fig. 5b). These results support an essential role of Drosha in the resolution of R-loops specifically at RPG loci. ChIP assays showed that the amount of RNAPII associated with the 3'-end of RPGs proximal to the transcription termination site was ~40% lower in *Drosha* KO cells compared in Ctrl cells (Fig. 5c). However, RNAPII association with the 5'-end of RPGs proximal to the TOP motif did not differ between Ctrl and *Drosha* KO cells (Supplementary Fig. S8), indicating that RNAPII elongation, but not RNAPII initiation, is affected by R-loop accumulation at RPG loci, leading to a reduced rate of transcription of RPGs.

Two observations led us to hypothesize that Ddx5 (an ATP-dependent RNA helicase) in association with Drosha might be required to resolve R-loops and promote RPG transcription. First, silencing of *Ddx5* caused a reduction in RPG mRNA abundance (Fig. 2f). Second, Ddx5 is implicated in the resolution of R-loops (60, 61). A ChIP assay confirmed the association of Ddx5 with RPG loci, which was Drosha-dependent because it was reduced in *Drosha* KO cells (Fig. 5d). Immunoprecipitation with the S9.6 antibody followed by immunoblot showed that a fraction of Ddx5—but not Drosha or Dgcr8—associated with R-loops (Fig. 5e, **Ctrl**). As seen with ChIP assays (Fig. 5d), the association of Ddx5 and R-loops was also reduced in *Drosha* KO cells (Fig. 5e), indicating that Ddx5 requires Drosha for R-loop interaction. A DRIP assay in K562 cells revealed that Ddx5 depletion increased the R-loops at RPG loci without affecting those on control loci (*Tubala* and *Tubb1*) (Fig. 5f). Together with the reduction in the amounts of Rps and Rpl mRNAs upon Ddx5 depletion (Fig. 2g), this result suggests that Ddx5 is required for the resolution of R-loops at RPG loci and to promote RPG transcription. When expressed at a level similar to endogenous Ddx5 in control HCT116 cells (Ctrl) containing Drosha, a RNA helicase-dead mutant of Ddx5 (Lys<sup>144</sup> to Asn; Ddx5 HD)(62) acted as a dominant negative and reduced the abundance of Rps and Rpl mRNAs (Fig. 5g and Supplementary Fig. S9), indicating that the RNA helicase activity of Ddx5 is required to facilitate RPG transcription. In cells in which *Drosha* was deleted by CRISPR/Cas9, the amount of Rps and Rpl mRNAs remained similar in cells expressing Ddx5 HD and Ddx5 WT (Fig. 5g), suggesting that Drosha and Ddx5 cooperatively regulate RPGs. Thus, these findings suggest that the Microprocessor complex facilitates R-loops resolution and RNAPII elongation.

### **Drosha is a critical modulator of RP biosynthesis upon changes in growth conditions**

Ribosome production is essential for fueling cell growth and proliferation, but its considerable energy costs require it to be tightly controlled and attuned to cellular growth conditions. The synchronized production of RPs permits the energy-efficient assembly of ribosomes (58) and is vital for the control of RP biosynthesis in line with cell proliferation (15, 58, 63). To test whether the Microprocessor complex plays a role in the change in RPG expression in response to the cellular growth environment, we cultured K562 cells under low (1%) or normal (10%) serum condition for 6 hr. The relative amounts of Rps19, Rps26, and Rpl11 were reduced by 59%, 84%, and 59%, respectively, under low serum conditions (Fig. 6a, **left and bottom right**). The transcripts for these RPs were also reduced in abundance (Fig. 6a, **top right**). Puromycin incorporation assays indicated that global protein synthesis was reduced by 30% and 50% in low serum for 6 hrs (Supplementary Fig. S10A) and 16 hrs (Supplementary Fig. S10B), respectively. We observed that the amount of Drosha protein, but not that of Dgcr8 or Ddx5, was decreased by 67% in cells cultured in low serum (Fig. 6a, **middle and bottom right**) without a corresponding change in *Drosha* mRNA abundance (Fig. 6a, **top right**). In control MEFs, both Rps24 and Rps26 proteins were reduced by 95% after nutrient starvation for 6 hr (Fig. 6b). Phosphorylated Rps6 (pRps6) was diminished upon nutrient starvation, which is indicative of inhibition of the mTOR-p70 S6 kinase pathway, and this effect was not rescued by exogenous expression of Flag-tagged Drosha did not rescue pRps6 depletion (Fig. 6b). However, the depletion of Rps24 and Rps26 by nutrient starvation was partially rescued by exogenous expression of Flag-Drosha (Fig. 6b). These results show that nutrient starvation reduces the amount of RPs by suppressing the



Microprocessor-dependent control of RP biogenesis independently of mTOR-dependent mechanisms (64).

### Drosha is degraded in a Nedd4-dependent manner upon serum starvation

Next, we addressed how Drosha abundance was decreased upon serum starvation. When *Nedd4* (*neural precursor cell expressed, developmentally downregulated 4*, also known as *Nedd4-1*) was depleted by siRNA, starvation-mediated reduction of Drosha and RPs was prevented (Fig. 7a). In contrast, silencing of *Nedd4L* (also known as *Nedd4-2*), a closely related member of the Nedd family of E3 ubiquitin ligases, did not rescue the degradation of Drosha upon serum starvation (Supplementary Fig. S11). We detected an interaction between Flag-Drosha and endogenous Nedd4 by immunoprecipitation (Fig. 7b). When Myc-tagged ubiquitin was expressed with Flag-Drosha in HEK293T cells, a small amount of poly-ubiquitinated Drosha was detected, which was increased 25-fold by overexpression of Nedd4 (Fig. 7c). Nedd4 contains WW domains that recognize the PPxY (PY) motif on its substrates (65). We noted that human Drosha contains an evolutionarily conserved PPGY sequence at amino acid 169–172, which is identical to the PY motif in the Nedd4 substrate Connexin 43 (66). When the PPGY sequence was mutated to AAGY in Drosha (AY mut), the ubiquitination of Drosha was reduced by 83%, indicating that the PY motif is required for the ubiquitination by Nedd4 (Fig. 7d). When K562 cells were serum starved for 6 hr and 16 hr, Nedd4 protein (Fig. 7e) increased 3.2-fold and 3.8-fold, respectively, without a corresponding change in *Nedd4* mRNA (Supplementary Fig. S12), indicating a post-transcriptional induction of Nedd4 upon serum starvation. In contrast with Nedd4, Drosha, Rps26, and Gata1 were decreased by 74%, 99%, and 44% after serum starvation for 16 hr, respectively (Fig. 7e), as expected. pRps6 was reduced by 23% and 86% after 6 hr and 16 hr serum starvation, respectively, confirming the inhibition of the mTOR-p70 S6 kinase pathway by serum starvation (Fig. 7e). To examine the subcellular localization of Drosha and Nedd4 upon serum starvation, we performed a nuclear/cytoplasmic fractionation of K562 cells. pRps6 and  $\beta$ -Tubulin segregated to cytoplasmic fractions whereas Lamin A/C appeared only in nuclear fractions, indicating a successful separation of the nuclear and cytoplasmic fractions (Fig. 7f). As expected, Drosha was predominantly localized in the nucleus under normal serum conditions (Fig. 7f). Although the total amount of Drosha gradually declined upon serum starvation, the cytoplasmic fraction of Drosha increased from 6% (no starvation) to 26% (6 hr low serum) and 48% (16 hr low serum) (Fig. 7f). Unlike Drosha, Nedd4 was predominantly in the cytoplasm, regardless of serum concentration (Fig. 7f). These results suggest that upon serum starvation, Drosha is exported from the nucleus and degraded by Nedd4 in the cytoplasm. Phosphorylation by p38 mitogen activated protein kinase (p38 MAPK) has been implicated in the nuclear export and subsequent degradation of Drosha upon oxidative stress and heat(67). Treatment with the p38 MAPK inhibitor SB203580 increased the nuclear fraction of Drosha from 52% to 77% under serum starvation (Fig. 7g), suggesting that Drosha nuclear export is mediated by p38 MAPK-dependent phosphorylation. Gata1 and Nedd4 remained in the nucleus and the cytoplasm, respectively, regardless of SB203580 treatment (Fig. 7g). Thus, we delineated a regulatory pathway connecting nutrient starvation to the p38-dependent export of Drosha from the nucleus into the cytoplasm, where Drosha is degraded through the action of Nedd4, which is moderately increased under starvation (Fig. 7h). This mechanism involving the subcellular

localization and protein stability of Drosha appears to play a key role in the control of ribosome abundance and global protein synthesis in response to a change in growth-promoting stimuli.

## Discussion

Drosha was originally characterized as an enzyme involved in rRNA maturation, based on the observed accumulation of 45S and 32S pre-rRNAs upon Drosha knockdown (68). In this study, we found that the Microprocessor complex mediates the coordinated synthesis of RP mRNAs in response to changes in the cellular environment. Thus, Drosha-mediated regulation of ribosome synthesis is twofold. A TOP motif that is functionally equivalent to that in RPGs can also be found in non-RP genes (non-ribosomal TOP genes) (15). The eCLIP data show that Drosha and DGCR8 associate with non-ribosomal TOP genes (Supplementary Fig. S6)(55). Quantitative mass-spectrometry analyses confirm that the expression of four *non-ribosomal TOP* genes—*EIF4B*, *PABPC1*, and *VIM*—requires Drosha, similarly to RPGs (Supplementary Fig. S4). Thus, the Microprocessor controls the synthesis of various components of the protein synthesis apparatus besides RPs (15). The ssRNA binding protein (RBP) LARP1 can bind the TOP motif of some RPG transcripts and facilitate their translation (22–27). However, LARP1 binds ~3,000 mRNAs, most of which do not contain a TOP motif (27). The impact of LARP1 on ribosome abundance and global protein synthesis, and its potential synergy with the Microprocessor on the regulation of RP synthesis, remain to be elucidated.

We have observed that nutrient deprivation promotes nuclear-to-cytoplasmic translocation of Drosha, followed by degradation by the cytoplasmic E3 ubiquitin ligase Nedd4. Nuclear-to-cytoplasmic shuttling of the Microprocessor complex and cleavage of viral RNAs upon viral infection has been reported as an antiviral mechanism, although the mechanism of regulation of the cytoplasmic shuttling of the Microprocessor upon viral infection is unknown(38, 69). Our results suggest that p38 MAPK-dependent phosphorylation of Drosha at Ser<sup>355</sup> contributes to the nuclear export of Drosha, as described in cells under oxidative or heat stress(67). Under these stresses, cells globally reduce new protein synthesis, except for a small subset of proteins that are essential for stress responses (70, 71). We propose that the p38 MAPK-Drosha-Nedd4 axis might mediate response to several cellular stresses, including starvation, oxidation and heat, which result in reduced protein synthesis. Unlike Ser<sup>355</sup> phosphorylation by p38 MAPK, phosphorylation at Ser<sup>300</sup> and Ser<sup>302</sup> by glycogen synthase kinase 3 $\beta$  (GSK3 $\beta$ ) is required for the nuclear retention of Drosha(72). Because GSK3 $\beta$  activity is regulated by various extracellular signals(73), it is possible that serum starvation might cause inhibition of GSK3 $\beta$  and promote the dephosphorylation of Ser<sup>300/302</sup> of Drosha, resulting in Drosha accumulation in the cytoplasm. An alternatively spliced form of Drosha without exon 6, which encodes the putative nuclear localization signal, is reported to localize in both the cytoplasm and the nucleus(74, 75). However, the molecular size of cytoplasmic Drosha after serum starvation is equivalent to full-length Drosha (159 kDa) and is indistinguishable from that of nuclear Drosha, making it unlikely that alternative splicing is involved in the change of nuclear/cytoplasmic ratio of Drosha upon serum starvation.

The transcriptional regulation of RPGs by Ddx5 through resolution of an R-loop is a new mechanism of regulation of ribosome biogenesis. The Microprocessor complex is reportedly recruited to DNA double strand break (DSB) sites, where it facilitates R-loop formation and promotes DSB repair (35). Thus, the Microprocessor may participate in both the formation and the resolution of R-loops, depending on the cellular context. In addition to Ddx5, RNA helicases—such as Dhx9, Ddx1, Ddx3x, Ddx15, Ddx17, Ddx18, Ddx21, Ddx27, Ddx39B, and Ddx54—have been identified to associate with DNA/RNA hybrids (60). Our study indicates that Ddx5 resolves R-loops at RPG loci to promote their transcription. Because there are 64 RNA helicases in human and 11 are found in association with the R-loops(60), we speculate that other RNA helicases might be recruited to different gene loci, where they promote or resolve R-loops depending on context, and thus participate in gene regulation similarly to Ddx5 and Dhx9.

Only 280 genes in yeast contain introns, and nearly half of them are RPGs. Yeast strains in which introns are deleted are unable to adapt to nutrient deprivation and die in part due to limited efficiency or availability of the spliceosome or of other RBPs and thus inhibition of the splicing of the RPG mRNAs (76, 77). Furthermore, nearly all genes in multicellular eukaryotes contain introns, and thus, an intronic RNA-dependent regulatory mechanism would be neither specific nor sufficient to provide a robust control over RP biogenesis. We propose that the Microprocessor-dependent transcriptional regulation of RPGs evolved in multicellular organisms as an alternative to intronic RNAs-mediated regulation of RPG transcripts in yeast. Both mechanisms involve a presumably ancient interaction between RNA and RBPs, whereas the abundance of RNA or RBPs is controlled by growth conditions.

Loss-of-function mutations in RPGs or in *Gata1* cause Diamond-Blackfan anemia (DBA; OMIM 105650)(1). In addition to anemia, DBA patients are short in stature and develop symptoms including arrhythmia, craniofacial defects, and thumb abnormalities of varying degrees of severity and penetrance(1). The tissue-specific manifestation of physical abnormalities in DBA suggests a cell-type specific differential susceptibility to ribosome abnormalities or insufficiency, presumably due to specific demands on protein synthesis. For example, we found that erythropoiesis is more severely impaired than vascular development in *Drosha* cKO mice (41, 78). We speculate that erythrocyte progenitors, which are rapidly proliferating and, therefore, have high demand for Gata1 and globin protein synthesis, are more susceptible to ribosome shortages than endothelial cells. Currently, only ~80% of DBA cases are accounted for by known gene mutations(1). Our study opens the possibility that the remaining DBA patients with no known gene mutations might carry hypomorphic alleles of the components of the Microprocessor.

## Materials and Methods

### Animal care and use

All animal experiments were conducted in accordance with the guidelines of the Institutional Animal Care and Use Committee (IACUC) at University of California, San Francisco. *Cdh5-Cre* line (79) and *Drosha*<sup>tm1Litt</sup> floxed line(80) have been previously described(41). Embryos were dated by the presence of vaginal plug in the female mouse as

embryonic day 0.5. The protocol number for the relevant animals and procedures approved by IACUC is AN185765-01: Title: Role of Growth Factor Signaling in Vascular Physiology” (Approval Date: July 27, 2020).

### Mouse genotyping

Genomic DNAs were isolated from tail tips or conceptus yolk sacs of postnatal day 12 pups and genotyped with regular PCR. Primers for genotyping and RT-PCR are listed in Supplementary Table S2.

### Flow cytometry and cell sorting

Flow cytometry and cell sorting were performed as described previously(41). Briefly, fetal liver, yolk sac or AGM was dissected from embryos and mechanically dissociated by pipetting into single cell suspension in Hank’s Balanced Salt Solution containing 2% fetal bovine serum (FBS), 1% penicillin/streptomycin and buffered with 10 mM HEPES, pH7.2 (FACS buffer). E10.5 embryos were collected in 200 ul FACS buffer, followed by a collection of peripheral blood. Cells were stained with fluorochrome conjugated antibody at 4°C for 1 hr, washed with DAPI (0.5 µg ml<sup>-1</sup>) containing FACS buffer and analyzed by FACS Verse (BD Biosciences) or sorted on a FACS Aria III (BD Biosciences) located at the UCSF FACS core. Data were analyzed with FlowJo v10.0.7. Single color stained samples were run with each flow cytometry analysis for compensation when analyzed with FlowJo. DAPI positive cells were gated out for analysis, then positive gating was applied when IgG staining sample was smaller than 0.1%.

### Antibodies

For Immunoblot, the following antibodies are used: Anti-Drosha antibody (1:500, Bethyl, A301-866A), anti-Dgcr8 (1:500, Proteintech,10996-1-AP), anti-Ddx5 (1:200, Abcam,ab21696), anti-GAPDH (1:5000, Millipore, MAB374), anti-Lamin A/C (1:2500, Cell signaling Technology, 2032), anti-Gata1 (1:200, R&D,MAB17791-SP), anti-γTubulin (1:5000, Santa Cruz Biotechnology, sc-7396), anti-puromycin (1:2000, Kerfast, 3RH11), anti-Rpl11 (1:300, Proteintech,16277-1-AP) anti-Rpsa (1:300, Abcam, ab137388), anti-Rps24 (1:300, Abcam, ab102986), anti-Rps26 (1:300, Abcam, ab104050), anti-Rps6 (1:500, Cell signaling Technology, 2317), anti-Rps19 (1:300, Santa Cruz Biotechnology, sc-100836), anti-β-actin (1:5000, Sigma-Aldrich, A5441), anti-NEDD4(1:2000, Cell signaling Technology, 2740), anti-Flag M2(1:2000, Sigma, F3165), anti-Myc (1:2500, Cell signaling Technology, 2278), anti-Myc-Tag (Cell signaling Technology, 2278), anti-RNA polymerase II (Millipore, 05-623), IRDye® 800CW Donkey anti-Rabbit IgG (H + L) (LI-COR, 926-32213), IRDye® 680RD Donkey anti-Mouse IgG (H + L) (LI-COR, 926-68072). For DRIP analysis, 10µg S9.6 (Millipore, MABE1095) antibody or normal mouse IgG (Santa Cruz, sc-2025) was used. For flow cytometry analysis or cell sorting, the following antibodies were used: PerCP anti-CD71 (1:200, BioLegend, 113815), FITC anti-Ter119 (1:200 BioLegend, 116205), PE anti-Itga4 (1:200, BioLegend,103607), Percp-IgG2bk (1:200, Biolegend 400336), FITC-IgG2ak (BD 553929), APC-IgG2bk (BD 556924), PE- IgG (Biolegend 405307), DAPI (ThermoFisher D1306).

## SDS-PAGE and immunoblotting analyses

SDS-PAGE and immunoblot analyses were performed as described previously(78).

## Cell culture

K562 cells were cultured in 10%FBS in RPMI1640 media (Corning 10-040-CV) supplemented with 200 $\mu$ M L-glutamine, 100  $\mu$ M sodium pyruvate and 1% penicillin/streptomycin at 37°C, 5% CO<sub>2</sub>. HCT116 cells, HEK293 or MEF cells were cultured in 10% FBS (Hyclone, SH3007103) in high glucose DMEM (Gibco 11965118) with 1% penicillin/streptomycin at 37°C, 5% CO<sub>2</sub>. To serum starve K562 cells, 1% FBS was used to replace 10% FBS in regular culture medium. To serum starve MEFs, HBSS (Thermo Fisher, 14025092) was used to replace the culture media.

## Colony formation unit (CFU) assay

CFU assay was performed as described previously(41). Briefly, E9.5 yolk sac was pipetted into single cell suspension which was seeded into methocult medium (Stem Cell Technologies M3434) and cultured for 7–10 days prior to counting the number of granulocyte-macrophage progenitors (GM), burst-forming unit erythroid (BFU-E), and granulocyte, erythrocyte, monocyte, megakaryocyte (GEMM) colonies.

## Quantitative reverse transcriptase-polymerase chain reaction (RT-PCR) analysis

Five ng of total RNA from CD71<sup>+</sup>Itga4<sup>+</sup> (*Drosha* cKO) or CD71<sup>+</sup>Itga4<sup>-</sup> (Ctrl) cells sorted from peripheral blood of E10.5 embryos were amplified and reverse transcribed with a Nugen ovation picoSL WTA system V2 (Nugen 3312–24). Amplified cDNAs were 100-times diluted. RT-PCR reactions were then performed in triplicate using iQ SYBR Green supermix (Bio-RAD 1708882). Primer sequences are listed in Supplementary Table S2.

## Retrovirus, lentivirus production and infection

Lenti-crispr *Drosha* V2 (gRNA for *Drosha*) and lenti-crispr NS V2(none-specific gRNA as control) were obtained from Dr. Graveley (University of Connecticut). pLKO.1-shDDX5 (Broadinstitute, TRCN00000113) and pLKO.1-scramble were also obtained from Dr. Graveley and used for generating lentivirus shDDX5 or scramble sh RNA. 15  $\mu$ g Lenti-crispr *Drosha* V2 or lenti-crispr NS V2, 7.5 $\mu$ g PMD2.G (Addgene plasmid #12259) and 7.5  $\mu$ g psPAX2 (Addgene plasmid #12260) were transfected into HEK293T cells seeded in a 15cm dish at 70% confluence by lipofectamine2000 (Invitrogen, 11668030) following manufacturer's manual. The media were replaced with DMED containing 10%FBS and high glucose 6 h after transfection. Lentivirus supernatant was collected after 48 h and filtered with 0.45 $\mu$ m filter. Lentivirus supernatant was aliquoted and stored at –80°C. Lentivirus was added to HCT116 or HEK293T cells at 30% confluency. Lentivirus containing media and culture media were mixed at 1:1 ratio. Polybrene was added to a final concentration of 8  $\mu$ g/ml. Cell culture media were replaced with the lentivirus and polybrene containing medium, grow in 5%CO<sub>2</sub> at 37°C overnight. The media were replaced with regular culture media. 48 h after infection, puromycin was added to the media at a final concentration of 5 ng/ $\mu$ l to select the lenti-virus infected cells. For retrovirus production, twenty  $\mu$ g pBABE-*Drosha* or pBABE, 10 $\mu$ g pVSVG (Addgene plasmid #8454) and 10  $\mu$ g psPAX2 (Addgene

plasmid #12260) were transfected to HEK293T cells seeded in a 15cm dish at 70% confluency. After changing the media, supernatant was collected, filtered with 0.45µm filter, aliquoted and stored at -80°C. MEFs were infected with viral supernatant in 2 µg/ml polybrene, and select with 5ng/µl puromycin.

### Plasmid construction

Human Drosha cDNA with a Flag-tag at the amino-terminus was cloned into *pBABE-puro* vector (Addgene plasmid#1764) for the production of retrovirus encoding human WT Drosha. Mouse *Ddx5 WT*(Addgene plasmid #88869) and the K144N mutant(Addgene plasmid #88870) were obtained from Addgene(62) . Ubiquitin\_Myc\_His plasmid is a gift from Dr. Jeff Wrana (Mount Sinai Hospital, Toronto). WT or mutant promoter of human *Rpl28* gene was cloned into *pGL-3-basic* (Promega, E1751). The Drosha RNA binding domain (RBD, 1259aa-1337aa) was cloned into *pCITE-2a* (Novagen TB050) for in vitro transcription translation assay. *pCI HA NEDD4* (Addgene plasmid #27002) was obtained from Addgene. Human Drosha cDNA with a Flag-tag at the amino-terminus and a 6x His tag at the carboxyl-terminus was cloned into *pcDNA4/TO* (Invitrogen) to construct the inducible WT Drosha expressing plasmid for immunoprecipitation assay and ubiquitination assay. R938N, K939A, and K940N mutations were generated in human Drosha to generate a ribonuclease-defective Drosha mutant (52).

### Chromatin immunoprecipitation (ChIP)

Flag-Drosha overexpressing MEFs and control MEFs (expressing the vector pBABE) were crosslinked treated with 2 mM disuccinimidyl glutarate (DSG; Thermo Fisher, 20593) at room temperature for 40 min. After MEFs were crosslinked with 1% Formaldehyde for 15 min at room temperature and quenched with 1M Glycine, cells were washed with PBS and lysed with lysis buffer (50 mM Tris-Cl pH 8.1, 10 mM EDTA, 1% SDS and protease inhibitor). Genomic DNAs were sheared to average length of 200–500bp by sonication, and lysates were cleared by centrifugation at 12,000g for 10 min at 4°C. Supernatants were incubated with protein A/G dynabeads (invitrogen 10002D) for 1 h at 4°C, diluted 1:10 with dilution buffer (20 mM Tris-Cl pH 8.1, 150 mM NaCl, 2 mM EDTA, 1% Triton X-100 and protease inhibitor) and incubated with M2 dynabeads (Sigma-Aldrich, M8823) for 40 h at 4°C. After dynabeads were washed with buffer I (20 mM Tris-Cl pH 8.1, 150 mM NaCl, 2 mM EDTA, 1% Triton X-100, 0.1% SDS), buffer II (20 mM Tris-Cl pH 8.1, 500 mM NaCl, 2 mM EDTA, 1% Triton X-100, 0.1% SDS), and buffer III (10mM Tris-Cl pH8.1, 250mM LiCl, 1mM EDTA, 1%NP-40, 1% Deoxycholate) at 4°C, the dynabeads were further washed twice with cold TE (10 mM Tris-Cl pH 8.1, 1 mM EDTA). The dynabeads were incubated in 250 µl elution buffer (200 mM NaHCO<sub>3</sub>, 1% SDS) at room temperature for 15 min twice. The eluates were mixed with 1/25 volume 5M NaCl and incubated at 65°C for 4 hr. 1/50 volume of 0.5 M EDTA, 1/25 volume of Tris-Cl pH 6.5, 1/100 volume of Proteinase K (10 mg/ml) were added and incubated at 45°C for 1 hr. Precipitated genome fragments were purified with QIAquick PCR Purification Kit and subjected to PCR analysis. 1µg/ml Actinomycin D (Sigma-Aldrich, A9415) was applied in the culture medium for 30 min before ChIP assay. RNaseA (Thermo Fisher, 12091021) was added into the lysed ChIP sample at a final concentration of 1µg/µl. RNase H(New England Biolab M0523S) was added into the lysed ChIP sample at a final concentration of 100U/ml. Primer sequences are

listed in Supplementary Table S2. For ChIP with anti-RNA polymerase II in K562 cells, crosslinking with DSG was omitted. Experimental procedures were the same as in MEFs except that K562 cells were crosslinked with 1% formaldehyde.

### Immunoprecipitation assay

293T cells were transfected with *pcDNA4-hDrosha* and *pCI HA NEDD4* or *pCI* vector. 2µg/ml doxycycline was added into medium to induce Drosha overexpression. 48 hr after transfection, cells were lysed in SBB buffer (1% Triton X-100, 150mM NaCl, 50mM Tris-Cl at pH 7.5, 1mM EDTA) supplemented with protease inhibitors (cOmplete, Roche-11836170001) and PhosStop (Roche-04906845001). Lysates were incubated at 4°C for 30 min and centrifuged at 12,000 g for 10 min at 4°C. Lysates were incubated with anti-Flag M2 Magnetic Beads (sigma, M8823) and rocked overnight at 4°C. M2 beads were washed in SBB buffer for 5 min at 4°C for three times, and boiled in sample buffer (Invitrogen, NP0007) with reducing agent (Invitrogen, NP0009).

### DNA/RNA hybrid Immunoprecipitation (DRIP) assay

K562 cells were lysed in digestion buffer (100 mM NaCl, 10mM Tris-Cl at pH 8, 25mM EDTA at pH 8, 0.5% SDS, 0.65 mg/ml protease K) at 55°C overnight. Lysates were mixed with 1 volume of phenol:chloroform:isoamyl alcohol (25:24:1, invitrogen, AM9722) and centrifuged at 12000 x g for 10 minutes at 4°C. Supernatant was transferred to a new tube. Lysates were again mixed with 1 volume of phenol:chloroform:isoamyl alcohol and centrifuged. The supernatant was precipitated with isopropanol. Half of the genomic DNA (gDNA) was subjected to RNase H (New England Biolabs, M0297) treatment at 5 µl per 30 µg gDNA in 200 µl final volume for 24 hr. After RNase H treatment, the gDNA were subjected to restriction enzyme digestion: MseI, DdeI, AluI and MboI at 5U/50µl for each enzyme, shaking at 37°C for 24 h or longer until the gDNA were cut into fragments with length of 100–500 bp. The digested gDNA were then incubated with 10 µg S9.6 antibody (Millipore MABE1095) or mouse nonspecific IgG (Santa Cruz Biotechnology, sc-2025) in DRIP binding buffer (10mM NaPO<sub>4</sub>, PH7.0, 140mM NaCl, 0.05% Triton-X-100) at 4°C for overnight. Protein A was added to samples, rotated at 4°C for 3 h, and washed with 1X DRIP binding buffer for four times at room temperature. The bead/antibody complexes were incubated with 0.5µg/µl Proteinase K for 40 min in a eppendorf ThermoMixer at 55°C, 1000 rpm. DNA was then extracted with 1 volume phenol:chloroform:isoamyl alcohol and precipitated with 1/10 volume 3M Sodium Acetate, 1µl glycogen (Invitrogen 10814010) and 2.5 volume ethanol. The DNA was then subjected to qPCR analysis.

### Cellular ubiquitin Assay

*pcDNA4-hDrosha*, *pCI HA NEDD4* or *Ubiquitin\_Myc\_His* plasmids were transfected into 293T cells at 30% confluence with lipofectamine 2000 (Invitrogen, 11668030) following the manufacturer's instructions. 2µg/ml doxycycline was added into medium to induce Drosha overexpression. 48 hours after transfection, cells of one 10 cm dish were lysed in 100 µl SBB buffer +1% SDS (1% Triton X-100, 150mM NaCl, 50mM Tris-Cl at pH 7.5, 1mM EDTA, 1% SDS) supplemented with protease inhibitors (cOmplete, Roche-11836170001) and PhosStop (Roche-04906845001), with rocking at 4°C for 30 min. Samples were then diluted with 900 µl SBB buffer, sonicated, rocked at 4°C for 30–60 min and centrifuged at

15000 g for 20 min. Supernatants were incubated with anti-Flag M2 Magnetic Beads (Sigma, M8823) and rocked overnight at 4°C. M2 beads were washed in SBB buffer for 5 min at 4°C for three times and boiled in sample buffer (Invitrogen, NP0007) with reducing agent (Invitrogen, NP0009).

### Sucrose gradient fractionation of polysomes

K562 cells (Ctrl and KO) were grown to a  $2 \times 10^5$  cells/ml confluency in the growth media. Cells were incubated with 100 µg/ml cycloheximide at 37°C for 5 min, collected by centrifugation, and re-suspended PBS+100 in µg/ml cycloheximide. Cells were pelleted again by centrifugation and lysed with three pellet-volumes ice cold hypotonic lysis buffer (10 mM HEPES pH 7.9, 1.5 mM MgCl<sub>2</sub>, 10 mM KCl, 0.5 mM DTT, 1% Triton X-100 and 100 µg/ml cycloheximide). After 10 min, cells were lysed on ice with ten strokes through a 26-gauge needle and nuclei were pelleted at 1,500× g for 5 min. Lysate from ~15 million cells was layered on top of 10–50% (w/v) sucrose gradients (20 mM HEPES:KOH pH 7.6, 100 mM KCl, 5 mM MgCl<sub>2</sub>, 1 mM DTT and 100 µg/ml cycloheximide) made using a Biocomp Instruments (Canada) gradient master. Gradients were centrifuged for 2 h at 36,000 RPM in a SW-41 rotor and manually peak fractionated using real-time A<sub>260</sub> monitoring with a Brandel (Gaithersburg, MD) gradient fractionator and ISCO (Lincoln, NE) UA-6 detector. Fractions were subjected to RNA prep with RNeasy Plus micro kit (Qiagen 74034) and a RT-PCR analysis with SYBR green (Biorad, 1725120).

### Quantitative mass spectrometry

K562 cells were infected with nonspecific or Droscha CRISPR lentivirus as described above with polybrene at a final concentration of 8 µg/ml. 48 hours after infection, K562 cells were selected with 2.5 ng/µl puromycin. Five replicates of each genotype were collected. iTRAQ-TMT mass spectrometry was performed using Q Exactive mass spectrometer (Thermo Fisher Scientific, USA) by Creative Proteomics, Inc on ten million cells for each replicate and 5 replicates per sample. The 6 raw MS files were analyzed and searched against human protein database based on the species of the samples using Maxquant (1.6.2.6). The parameters were set as follows. The protein modifications were carbamidomethylation (C) (fixed), oxidation (M) (variable); the enzyme specificity was set to trypsin; the maximum missed cleavages were set to 2; the precursor ion mass tolerance was set to 10 ppm, and MS/MS tolerance was 0.6 Da. Only high confidence identified peptides were chosen for downstream protein identification analysis. Data are available in Data File S1.

### Next Generation RNA-sequencing and high-throughput data analysis

Erythroblast cells (CD71<sup>high</sup>Ter119<sup>+</sup>) from the peripheral blood of 5 E10.5 Ctrl embryos with genotype of *Droscha*<sup>fl/+</sup>; *Cdh5-cre*<sup>+</sup> or *Droscha*<sup>fl/fl</sup>, or *Droscha*<sup>fl/+</sup> and five cKO embryos with genotype of *Droscha*<sup>fl/fl</sup>; *Cdh5-cre*<sup>+</sup> were sorted on a FACS Aria III (BD Biosciences) located at the UCSF FACS core. RNA was prepared from the samples with an RNeasy Plus micro kit (Qiagen 74034). The quality of RNAs was evaluated with 2100 Bioanalyzer Instrument (Agilent Technologies). RNA samples with RIN>8.0 were shipped to Beijing Genome Institute for library preparation and sequencing (Illumina HiSeq 2500). Around 70 million reads were obtained for each pooled sample. Gene Ontology (GO) term enrichment was performed using the set of downregulated genes in RNA-seq, defined as genes with log<sub>2</sub>



(cKO/Ctrl) $<-0.6$  with clusterProfiler package in R(81). Fastq files for DRIP-seq were downloaded from GEO datasets (GSE97648) and aligned to the human genome(GRCh38) using bowtie2-2.3.4.1(35). Integrative Genomics Viewer (2.4.14 Broad Institute) was used for data analysis. Metagene analysis was done using the Bioconductor metagene2 package (R package version 1.4.0, <https://github.com/ArnaudDroitLab/metagene2>). Specifically, the Drosha eCLIP datasets (Homo sapiens K562 cells) were downloaded from GEO:GSE91954 and GEO:GSE92088 (55) and bam files aligned to hg19 reference were used for analysis. Two thousand bp downstream of the transcription starting sites of all genes and RPGs were used for comparison. Mean coverage was calculated across 20 bp bins and the 95% confidence interval were calculated with 1000 bootstrap samplings. Venn diagrams were drawn with the online tool (<https://www.stefanjol.nl/venny>). ChIP-seq peaks were called using MACS version 1.4.2. (model-based analysis of ChIP-seq)(53). The source of the high-throughput sequence data are listed in Supplementary Table 1.

### Puromycin incorporation assay

For in vivo puromycin incorporation, puromycin (0.04  $\mu\text{mol/g}$  body weight) was injected into E11.5 pregnant mice intraperitoneally 35 min before embryos were harvested. Erythroid progenitors (CD71<sup>+</sup>Ter119<sup>+</sup>) were isolated by flow cytometry from the peripheral blood of embryos, homogenized, and immunoblotted with a puromycin antibody. For in vitro puromycin incorporation in K562 cells, after serum starvation for 16 h, 1  $\mu\text{mol/l}$  puromycin was added to the culture media for 10 min. Total cell lysates were generated from  $5 \times 10^6$  cells from 1% or 10% serum treated K562 cells and subjected to immunoblotting with a puromycin antibody (Kerafast, #EQ0001).

### Electrophoretic mobility shift assay (EMSA)

100 pmol of WT or mutant RNA oligonucleotides (synthesized by Integrated DNA Technologies, Inc.) were 5'-end labeled with [ $\gamma$ -<sup>32</sup>P] ATP (Perkin Elmer, NEG035C001MC) and T4 polynucleotide kinase (New England Biolabs) as previously described (82). Unincorporated ATP was removed by Illustra MicroSpin G-25 Columns (GE Healthcare Life Sciences, UK). The radiolabeled RNA probe was denatured in buffer (50 mM Tris-Cl ; 100 mM KCl; 2.5 mM MgCl<sub>2</sub>; 100 mM NaCl) at 72°C, and then renatured gradually at a rate of 1°C/min. EMSA was performed by incubating the radiolabeled probe (100,000 cpm) with Drosha RBD protein, which was synthesized in vitro with a reticulocyte lysate system (Promega, L5020), for 2 h at room temperature in binding buffer (50 mM Tris-Cl, pH 7.5; 100 mM KCl; 2.5 mM MgCl<sub>2</sub>; 100 mM NaCl; 0.01% NP-40; 1 mM DTT; 5% glycerol; 10  $\mu\text{g/ml}$  bovine serum albumin; 0.1mg/ml sperm DNA) (82). The RNA-protein mixtures were then electrophoresed in 8% acrylamide-TBE gels. Gels were dried and exposed to X-ray film for analysis. For the competition experiments, the proteins were incubated with labeled WT RNA and 50-fold molar excess of the unlabeled WT or mutated single-stranded RNA at room temperature for 2 hours before electrophoresis.

### Luciferase constructs and assay

The promoter area of human *Rpl28* gene was cloned at HindIII/NcoI site of the pGL3-basic (Promega, E1751) to make pGL3-reporters. *pGL3-reporter*, *pGL3-basic* (400 ng each), and *renilla luciferase* expression plasmid (1 ng) were transfected into HEK293 cells or HCT116

cells by lipofectamine2000 (Invitrogen, 11668030) following the manufacturer's manual. 48 h after transfection, total cell lysates were prepared and subjected to the luciferase assay as described(83). Firefly luciferase activity was normalized to renilla luciferase activity to normalize transfection efficiency.

### Statistical analysis

Graphs were generated with GraphPad PRISM software. Statistical significance was calculated in R version 3.2.3 by Student's t test. The null hypothesis of the medians/means being equal was rejected at  $\alpha = 0.05$  and p values were generated by unpaired Student's t test and presented in figures. The sample size was estimated by power analysis and is presented in the figure legend. The investigators were blinded during experiments because genotyping was performed after experiments. No animals were excluded, and animals were allocated based on genotype. Cells for experiments were randomized. For animal analysis, at least three animals were used in each experiment and all experiments were completed in gender- and genotype-blinded manner. All the other experiments were performed at least three times with biological triplicates each time. For PCR analysis, each biological sample was analyzed with a specific primer set in triplicate each time.

### Supplementary Material

Refer to Web version on PubMed Central for supplementary material.

### Acknowledgments

We thank Kyle Soo, Bryn Sullivan and Armita Norouzi for contributing to the research. We thank Dr. Brenton Graveley (University of Connecticut) for Lenti-Crispr-Drosha and Lenti-Crispr-NS constructs, Dr. Robert Blelloch for *Dgcr8*<sup>-/-</sup> mES cells, and Dr. Narry V. Kim (Seoul National University) for the Drosha RKK/QAQ mutant construct.

#### Funding

This study was funded by NIH HL132058 to A.H, DK119621 to B.L.B., the UCSF Program for Breakthrough Biomedical Research, funded in part by the Sandler Foundation to S.N.F, the California Tobacco-Related Disease Research Grants Program 27KT-0003 to S.N.F, and the National Institutes of Health DP2GM132932 to S.N.F. X.J. was supported by NIH T32 training grant to B.L.B.

### References and Notes

1. Ludwig LS, Gazda HT, Eng JC, Eichhorn SW, Thiru P, Ghazvinian R, George TI, Gotlib JR, Beggs AH, Sieff CA, Lodish HF, Lander ES, and Sankaran VG, Altered translation of GATA1 in Diamond-Blackfan anemia. *Nat Med*, 2014. 20(7): 748–53. [PubMed: 24952648]
2. Genuth NR and Barna M, Heterogeneity and specialized functions of translation machinery: from genes to organisms. *Nat Rev Genet*, 2018. 19(7): 431–452. [PubMed: 29725087]
3. Nomura M, Gourse R, and Baughman G, Regulation of the synthesis of ribosomes and ribosomal components. *Annu Rev Biochem*, 1984. 53: 75–117. [PubMed: 6206783]
4. Zengel JM and Lindahl L, Diverse mechanisms for regulating ribosomal protein synthesis in *Escherichia coli*. *Prog Nucleic Acid Res Mol Biol*, 1994. 47: 331–70. [PubMed: 7517053]
5. Simsek D and Barna M, An emerging role for the ribosome as a nexus for post-translational modifications. *Curr Opin Cell Biol*, 2017. 45: 92–101. [PubMed: 28445788]
6. Leppek K, Das R, and Barna M, Functional 5' UTR mRNA structures in eukaryotic translation regulation and how to find them. *Nat Rev Mol Cell Biol*, 2018. 19(3): 158–174. [PubMed: 29165424]

7. Warner JR, The economics of ribosome biosynthesis in yeast. *Trends Biochem Sci*, 1999. 24(11): 437–40. [PubMed: 10542411]
8. Lieb JD, Liu X, Botstein D, and Brown PO, Promoter-specific binding of Rap1 revealed by genome-wide maps of protein-DNA association. *Nat Genet*, 2001. 28(4): 327–34. [PubMed: 11455386]
9. Martin DE, Soulard A, and Hall MN, TOR regulates ribosomal protein gene expression via PKA and the Forkhead transcription factor FHL1. *Cell*, 2004. 119(7): 969–79. [PubMed: 15620355]
10. Rudra D, Zhao Y, and Warner JR, Central role of Ifh1p-Fhl1p interaction in the synthesis of yeast ribosomal proteins. *EMBO J*, 2005. 24(3): 533–42. [PubMed: 15692568]
11. Schawalder SB, Kabani M, Howald I, Choudhury U, Werner M, and Shore D, Growth-regulated recruitment of the essential yeast ribosomal protein gene activator Ifh1. *Nature*, 2004. 432(7020): 1058–61. [PubMed: 15616569]
12. Wade JT, Hall DB, and Struhl K, The transcription factor Ifh1 is a key regulator of yeast ribosomal protein genes. *Nature*, 2004. 432(7020): 1054–8. [PubMed: 15616568]
13. Warner JR and McIntosh KB, How common are extraribosomal functions of ribosomal proteins? *Mol Cell*, 2009. 34(1): 3–11. [PubMed: 19362532]
14. Gabunilas J and Chanfreau G, Splicing-Mediated Autoregulation Modulates Rpl22p Expression in *Saccharomyces cerevisiae*. *PLoS Genet*, 2016. 12(4): e1005999.
15. Meyuhas O and Kahan T, The race to decipher the top secrets of TOP mRNAs. *Biochim Biophys Acta*, 2015. 1849(7): 801–11. [PubMed: 25234618]
16. Jefferies HB, Reinhard C, Kozma SC, and Thomas G, Rapamycin selectively represses translation of the “polypyrimidine tract” mRNA family. *Proc Natl Acad Sci U S A*, 1994. 91(10): 4441–5. [PubMed: 8183928]
17. Thoreen CC, Chantranupong L, Keys HR, Wang T, Gray NS, and Sabatini DM, A unifying model for mTORC1-mediated regulation of mRNA translation. *Nature*, 2012. 485(7396): 109–13. [PubMed: 22552098]
18. Pellizzoni L, Lotti F, Maras B, and Pierandrei-Amaldi P, Cellular nucleic acid binding protein binds a conserved region of the 5' UTR of *Xenopus laevis* ribosomal protein mRNAs. *J Mol Biol*, 1997. 267(2): 264–75. [PubMed: 9096224]
19. Huichalaf C, Schoser B, Schneider-Gold C, Jin B, Sarkar P, and Timchenko L, Reduction of the rate of protein translation in patients with myotonic dystrophy 2. *J Neurosci*, 2009. 29(28): 9042–9. [PubMed: 19605641]
20. Avni D, Shama S, Loreni F, and Meyuhas O, Vertebrate mRNAs with a 5'-terminal pyrimidine tract are candidates for translational repression in quiescent cells: characterization of the translational cis-regulatory element. *Mol Cell Biol*, 1994. 14(6): 3822–33. [PubMed: 8196625]
21. Damgaard CK and Lykke-Andersen J, Translational coregulation of 5'TOP mRNAs by TIA-1 and TIAR. *Genes Dev*, 2011. 25(19): 2057–68. [PubMed: 21979918]
22. Philippe L, Vasseur JJ, Debart F, and Thoreen CC, La-related protein 1 (LARP1) repression of TOP mRNA translation is mediated through its cap-binding domain and controlled by an adjacent regulatory region. *Nucleic Acids Res*, 2018. 46(3): 1457–1469. [PubMed: 29244122]
23. Lahr RM, Fonseca BD, Ciotti GE, Al-Ashtal HA, Jia JJ, Niklaus MR, Blagden SP, Alain T, and Berman AJ, La-related protein 1 (LARP1) binds the mRNA cap, blocking eIF4F assembly on TOP mRNAs. *Elife*, 2017. 6.
24. Tcherkezian J, Cargnello M, Romeo Y, Huttlin EL, Lavoie G, Gygi SP, and Roux PP, Proteomic analysis of cap-dependent translation identifies LARP1 as a key regulator of 5'TOP mRNA translation. *Genes Dev*, 2014. 28(4): 357–71. [PubMed: 24532714]
25. Fonseca BD, Zakaria C, Jia JJ, Graber TE, Svitkin Y, Tahmasebi S, Healy D, Hoang HD, Jensen JM, Diao IT, Lussier A, Dajadian C, Padmanabhan N, Wang W, Matta-Camacho E, Hearnden J, Smith EM, Tsukumo Y, Yanagiya A, Morita M, Petroulakis E, González JL, Hernández G, Alain T, and Damgaard CK, La-related Protein 1 (LARP1) Represses Terminal Oligopyrimidine (TOP) mRNA Translation Downstream of mTOR Complex 1 (mTORC1). *J Biol Chem*, 2015. 290(26): 15996–6020.
26. Hong S, Freeberg MA, Han T, Kamath A, Yao Y, Fukuda T, Suzuki T, Kim JK, and Inoki K, LARP1 functions as a molecular switch for mTORC1-mediated translation of an essential class of mRNAs. *Elife*, 2017. 6.

27. Mura M, Hopkins TG, Michael T, Abd-Latip N, Weir J, Aboagye E, Mauri F, Jameson C, Sturge J, Gabra H, Bushell M, Willis AE, Curry E, and Blagden SP, LARP1 post-transcriptionally regulates mTOR and contributes to cancer progression. *Oncogene*, 2015. 34(39): 5025–36. [PubMed: 25531318]
28. Orom UA, Nielsen FC, and Lund AH, MicroRNA-10a binds the 5'UTR of ribosomal protein mRNAs and enhances their translation. *Mol Cell*, 2008. 30(4): 460–71. [PubMed: 18498749]
29. Siomi H and Siomi MC, Posttranscriptional regulation of microRNA biogenesis in animals. *Mol Cell*, 2010. 38(3): 323–32. [PubMed: 20471939]
30. Hata A and Lieberman J, Dysregulation of microRNA biogenesis and gene silencing in cancer. *Sci Signal*, 2015. 8(368): re3.
31. Kim B, Jeong K, and Kim VN, Genome-wide Mapping of DROSHA Cleavage Sites on Primary MicroRNAs and Noncanonical Substrates. *Mol Cell*, 2017. 66(2): 258–269.e5.
32. Han J, Pedersen JS, Kwon SC, Belair CD, Kim YK, Yeom KH, Yang WY, Haussler D, Blelloch R, and Kim VN, Posttranscriptional crossregulation between Drosha and DGCR8. *Cell*, 2009. 136(1): 75–84. [PubMed: 19135890]
33. Oskowitz AZ, Penformis P, Tucker A, Prockop DJ, and Pochampally R, Drosha regulates hMSCs cell cycle progression through a miRNA independent mechanism. *Int J Biochem Cell Biol*, 2011. 43(11): 1563–72. [PubMed: 21794839]
34. Gromak N, Dienstbier M, Macias S, Plass M, Eyraas E, Cáceres JF, and Proudfoot NJ, Drosha regulates gene expression independently of RNA cleavage function. *Cell Rep*, 2013. 5(6): 1499–510. [PubMed: 24360955]
35. Lu WT, Hawley BR, Skalka GL, Baldock RA, Smith EM, Bader AS, Malewicz M, Watts FZ, Wilczynska A, and Bushell M, Drosha drives the formation of DNA:RNA hybrids around DNA break sites to facilitate DNA repair. *Nat Commun*, 2018. 9(1): 532. [PubMed: 29416038]
36. Francia S, Michelini F, Saxena A, Tang D, de Hoon M, Anelli V, Mione M, Carninci P, and d'Adda di Fagagna F, Site-specific DICER and DROSHA RNA products control the DNA-damage response. *Nature*, 2012. 488(7410): 231–5. [PubMed: 22722852]
37. Francia S, Cabrini M, Matti V, Oldani A, and d'Adda di Fagagna F, DICER, DROSHA and DNA damage response RNAs are necessary for the secondary recruitment of DNA damage response factors. *J Cell Sci*, 2016. 129(7): 1468–76. [PubMed: 26906421]
38. Shapiro JS, Schmid S, Aguado LC, Sabin LR, Yasunaga A, Shim JV, Sachs D, Cherry S, and tenOever BR, Drosha as an interferon-independent antiviral factor. *Proc Natl Acad Sci U S A*, 2014. 111(19): 7108–13. [PubMed: 24778219]
39. Aguado LC, Schmid S, May J, Sabin LR, Panis M, Blanco-Melo D, Shim JV, Sachs D, Cherry S, Simon AE, Levraud JP, and tenOever BR, RNase III nucleases from diverse kingdoms serve as antiviral effectors. *Nature*, 2017. 547(7661): 114–117. [PubMed: 28658212]
40. García-Muse T and Aguilera A, R Loops: From Physiological to Pathological Roles. *Cell*, 2019. 179(3): 604–618. [PubMed: 31607512]
41. Jiang X, Hawkins JS, Lee J, Lizama CO, Bos FL, Zape JP, Ghatpande P, Peng Y, Louie J, Lagna G, Zovein AC, and Hata A, Let-7 microRNA-dependent control of leukotriene signaling regulates the transition of hematopoietic niche in mice. *Nat Commun*, 2017. 8(1): 128. [PubMed: 28743859]
42. Koulunis M, Pop R, Porpiglia E, Shearstone JR, Hidalgo D, and Socolovsky M, Identification and analysis of mouse erythroid progenitors using the CD71/TER119 flow-cytometric assay. *J Vis Exp*, 2011(54).
43. Suzuki M, Shimizu R, and Yamamoto M, Transcriptional regulation by GATA1 and GATA2 during erythropoiesis. *Int J Hematol*, 2011. 93(2): 150–155. [PubMed: 21279818]
44. Pevny L, Lin CS, D'Agati V, Simon MC, Orkin SH, and Costantini F, Development of hematopoietic cells lacking transcription factor GATA-1. *Development*, 1995. 121(1): 163–72. [PubMed: 7867497]
45. Campbell AE, Wilkinson-White L, Mackay JP, Matthews JM, and Blobel GA, Analysis of disease-causing GATA1 mutations in murine gene complementation systems. *Blood*, 2013. 121(26): 5218–27. [PubMed: 23704091]

46. Patrick DM, Zhang CC, Tao Y, Yao H, Qi X, Schwartz RJ, Jun-Shen Huang L, and Olson EN, Defective erythroid differentiation in miR-451 mutant mice mediated by 14–3-3zeta. *Genes Dev*, 2010. 24(15): 1614–9. [PubMed: 20679397]
47. Tomoda T, Kurashige T, Yamamoto H, Fujimoto S, and Taniguchi T, Fluctuation of gene expression for poly(ADP-ribose) synthetase during hemin-induced erythroid differentiation of human leukemia K562 cells and its reversion process. *Biochim Biophys Acta*, 1991. 1088(3): 359–64. [PubMed: 1901731]
48. Aviner R, Geiger T, and Elroy-Stein O, Novel proteomic approach (PUNCH-P) reveals cell cycle-specific fluctuations in mRNA translation. *Genes Dev*, 2013. 27(16): 1834–44. [PubMed: 23934657]
49. Kim YK, Kim B, and Kim VN, Re-evaluation of the roles of DROSHA, Exportin 5, and DICER in microRNA biogenesis. *Proc Natl Acad Sci U S A*, 2016. 113(13): E1881–9.
50. Chen X, Wang L, Huang R, Qiu H, Wang P, Wu D, Zhu Y, Ming J, Wang Y, Wang J, and Na J, Dgcr8 deletion in the primitive heart uncovered novel microRNA regulating the balance of cardiac-vascular gene program. *Protein Cell*, 2019. 10(5): 327–346. [PubMed: 30128894]
51. Davis CA, Hitz BC, Sloan CA, Chan ET, Davidson JM, Gabdank I, Hilton JA, Jain K, Baymuradov UK, Narayanan AK, Onate KC, Graham K, Miyasato SR, Dreszer TR, Strattan JS, Jolanki O, Tanaka FY, and Cherry JM, The Encyclopedia of DNA elements (ENCODE): data portal update. *Nucleic Acids Res*, 2018. 46(D1): D794–D801. [PubMed: 29126249]
52. Kwon SC, Nguyen TA, Choi YG, Jo MH, Hohng S, Kim VN, and Woo JS, Structure of Human DROSHA. *Cell*, 2016. 164(1–2): 81–90. [PubMed: 26748718]
53. Suzuki HI, Young RA, and Sharp PA, Super-Enhancer-Mediated RNA Processing Revealed by Integrative MicroRNA Network Analysis. *Cell*, 2017. 168(6): 1000–1014 e15.
54. Gromak N, Dienstbier M, Macias S, Plass M, Eyraes E, Cáceres JF, and Proudfoot NJ, Drosha Regulates Gene Expression Independently of RNA Cleavage Function. *Cell Rep*, 2014. 7(5): 1753–1754. [PubMed: 28903032]
55. Van Nostrand EL, Pratt GA, Yee BA, Wheeler EC, Blue SM, Mueller J, Park SS, Garcia KE, Gelboin-Burkhart C, Nguyen TB, Rabano I, Stanton R, Sundararaman B, Wang R, Fu XD, Graveley BR, and Yeo GW, Principles of RNA processing from analysis of enhanced CLIP maps for 150 RNA binding proteins. *Genome Biol*, 2020. 21(1): 90. [PubMed: 32252787]
56. Perina D, Korolija M, Roller M, Harcet M, Jelić B, Miko A, and Cetković H, Over-represented localized sequence motifs in ribosomal protein gene promoters of basal metazoans. *Genomics*, 2011. 98(1): 56–63. [PubMed: 21457775]
57. Rojas DA, Moreira-Ramos S, Urbina F, and Maldonado E, Transcriptional regulation of ribosomal protein genes in yeast and metazoan cells. *J. Mol. Cell. Biochem*, 2018. 2(1): 1–6.
58. Hamilton TL, Stoneley M, Spriggs KA, and Bushell M, TOPs and their regulation. *Biochem Soc Trans*, 2006. 34(Pt 1): 12–6. [PubMed: 16246169]
59. Lopez-Carballo G, Moreno L, Masia S, Perez P, and Baretino D, Activation of the phosphatidylinositol 3-kinase/Akt signaling pathway by retinoic acid is required for neural differentiation of SH-SY5Y human neuroblastoma cells. *J Biol Chem*, 2002. 277(28): 25297–304.
60. Cristini A, Groh M, Kristiansen MS, and Gromak N, RNA/DNA Hybrid Interactome Identifies DXH9 as a Molecular Player in Transcriptional Termination and R-Loop-Associated DNA Damage. *Cell Rep*, 2018. 23(6): 1891–1905. [PubMed: 29742442]
61. Mersaoui SY, Yu Z, Coulombe Y, Karam M, Busatto FF, Masson JY, and Richard S, Arginine methylation of the DDX5 helicase RGG/RG motif by PRMT5 regulates resolution of RNA:DNA hybrids. *EMBO J*, 2019. 38(15): e100986.
62. Huang W, Thomas B, Flynn RA, Gavzy SJ, Wu L, Kim SV, Hall JA, Miraldi ER, Ng CP, Rigo F, Rigo FW, Meadows S, Montoya NR, Herrera NG, Domingos AI, Rastinejad F, Myers RM, Fuller-Pace FV, Bonneau R, Chang HY, Acuto O, and Littman DR, DDX5 and its associated lncRNA Rmrp modulate TH17 cell effector functions. *Nature*, 2015. 528(7583): 517–22. [PubMed: 26675721]
63. Patursky-Polischuk I, Kasir J, Miloslavski R, Hayouka Z, Hausner-Hanochi M, Stolovich-Rain M, Tsukerman P, Biton M, Mudhasani R, Jones SN, and Meyuhos O, Reassessment of the role of

TSC, mTORC1 and microRNAs in amino acids-mediated translational control of TOP mRNAs. *PLoS One*, 2014. 9(10): e109410.

64. Gentilella A, Kozma SC, and Thomas G, A liaison between mTOR signaling, ribosome biogenesis and cancer. *Biochim Biophys Acta*, 2015. 1849(7): 812–20. [PubMed: 25735853]
65. Huang X, Chen J, Cao W, Yang L, Chen Q, He J, Yi Q, Huang H, Zhang E, and Cai Z, The many substrates and functions of NEDD4–1. *Cell Death Dis*, 2019. 10(12): 904. [PubMed: 31787758]
66. Spagnol G, Kieken F, Kopanic JL, Li H, Zach S, Stauch KL, Grosely R, and Sorgen PL, Structural Studies of the Nedd4 WW Domains and Their Selectivity for the Connexin43 (Cx43) Carboxyl Terminus. *J Biol Chem*, 2016. 291(14): 7637–50. [PubMed: 26841867]
67. Yang Q, Li W, She H, Dou J, Duong DM, Du Y, Yang SH, Seyfried NT, Fu H, Gao G, and Mao Z, Stress induces p38 MAPK-mediated phosphorylation and inhibition of Drosha-dependent cell survival. *Mol Cell*, 2015. 57(4): 721–734. [PubMed: 25699712]
68. Wu H, Xu H, Miraglia LJ, and Crooke ST, Human RNase III is a 160-kDa protein involved in preribosomal RNA processing. *J Biol Chem*, 2000. 275(47): 36957–65.
69. Shapiro JS, Langlois RA, Pham AM, and Tenoever BR, Evidence for a cytoplasmic microprocessor of pri-miRNAs. *RNA*, 2012. 18(7): 1338–46. [PubMed: 22635403]
70. Reichmann D, Voth W, and Jakob U, Maintaining a Healthy Proteome during Oxidative Stress. *Mol Cell*, 2018. 69(2): 203–213. [PubMed: 29351842]
71. Duncan RF and Hershey JW, Protein synthesis and protein phosphorylation during heat stress, recovery, and adaptation. *J Cell Biol*, 1989. 109(4 Pt 1): 1467–81. [PubMed: 2793930]
72. Tang X, Li M, Tucker L, and Ramratnam B, Glycogen synthase kinase 3 beta (GSK3beta) phosphorylates the RNAase III enzyme Drosha at S300 and S302. *PLoS One*, 2011. 6(6): e20391.
73. Beurel E, Grieco SF, and Jope RS, Glycogen synthase kinase-3 (GSK3): regulation, actions, and diseases. *Pharmacol Ther*, 2015. 148: 114–31. [PubMed: 25435019]
74. Dai L, Chen K, Youngren B, Kulina J, Yang A, Guo Z, Li J, Yu P, and Gu S, Cytoplasmic Drosha activity generated by alternative splicing. *Nucleic Acids Res*, 2016. 44(21): 10454–10466.
75. Link S, Grund SE, and Diederichs S, Alternative splicing affects the subcellular localization of Drosha. *Nucleic Acids Res*, 2016. 44(11): 5330–43. [PubMed: 27185895]
76. Morgan JT, Fink GR, and Bartel DP, Excised linear introns regulate growth in yeast. *Nature*, 2019. 565(7741): 606–611. [PubMed: 30651636]
77. Parenteau J, Maignon L, Berthoumieux M, Catala M, Gagnon V, and Abou Elela S, Introns are mediators of cell response to starvation. *Nature*, 2019. 565(7741): 612–617. [PubMed: 30651641]
78. Jiang X, Wooderchak-Donahue WL, McDonald J, Ghatpande P, Baalbaki M, Sandoval M, Hart D, Clay H, Coughlin S, Lagna G, Bayrak-Toydemir P, and Hata A, Inactivating mutations in Drosha mediate vascular abnormalities similar to hereditary hemorrhagic telangiectasia. *Sci Signal*, 2018. 11(513).
79. Chen MJ, Yokomizo T, Zeigler BM, Dzierzak E, and Speck NA, Runx1 is required for the endothelial to haematopoietic cell transition but not thereafter. *Nature*, 2009. 457(7231): 887–91. [PubMed: 19129762]
80. Chong MM, Rasmussen JP, Rudensky AY, and Littman DR, The RNaseIII enzyme Drosha is critical in T cells for preventing lethal inflammatory disease. *J Exp Med*, 2008. 205(9): 2005–17. [PubMed: 18725527]
81. Yu G, Wang LG, Han Y, and He QY, clusterProfiler: an R package for comparing biological themes among gene clusters. *OMICS*, 2012. 16(5): 284–7. [PubMed: 22455463]
82. Celona B, Dollen JV, Vatsavayai SC, Kashima R, Johnson JR, Tang AA, Hata A, Miller BL, Huang EJ, Krogan NJ, Seeley WW, and Black BL, Suppression of C9orf72 RNA repeat-induced neurotoxicity by the ALS-associated RNA-binding protein Zfp106. *Elife*, 2017. 6.
83. Chang J, Davis-Dusenbery BN, Kashima R, Jiang X, Marathe N, Sessa R, Louie J, Gu W, Lagna G, and Hata A, Acetylation of p53 stimulates miRNA processing and determines cell survival following genotoxic stress. *EMBO J*, 2013. 32(24): 3192–205. [PubMed: 24219989]
84. Pope BD, Ryba T, Dileep V, Yue F, Wu W, Denas O, Vera DL, Wang Y, Hansen RS, Canfield TK, Thurman RE, Cheng Y, Gulsoy G, Dennis JH, Snyder MP, Stamatoyannopoulos JA, Taylor J, Hardison RC, Kahveci T, Ren B, and Gilbert DM, Topologically associating domains are stable units of replication-timing regulation. *Nature*, 2014. 515(7527): 402–5. [PubMed: 25409831]

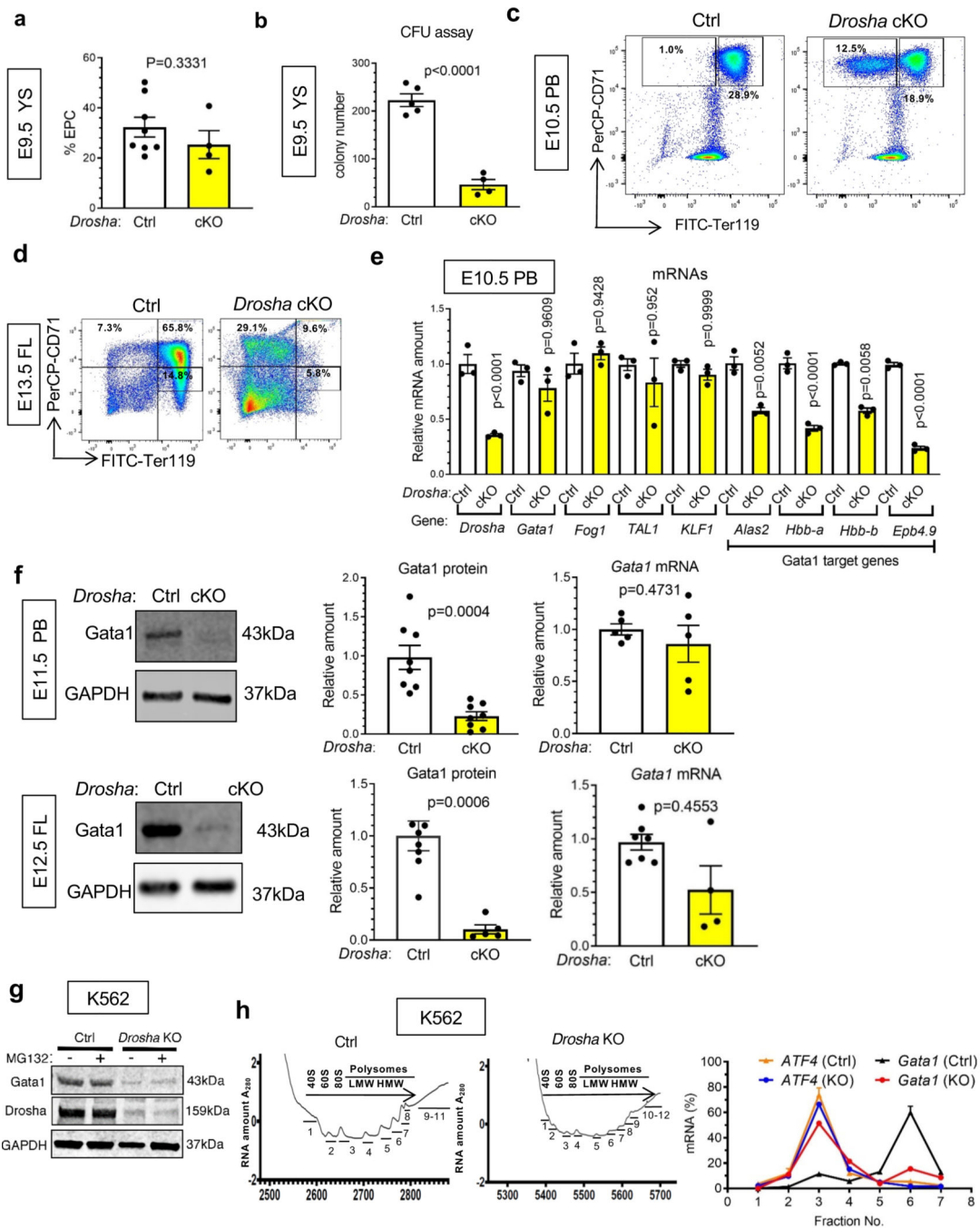


**Fig. 1. Endothelial-specific deletion of mouse *Drosha* impairs erythropoiesis.**

**a.** Quantification of frequency (%) of total live (DAPI<sup>-</sup>) erythroblasts (CD71<sup>+</sup>) derived from E9.5 yolk sac (YS) by flow cytometry (means ± SEM). NS, not significant (two-tailed unpaired Student's t test). n=8 Ctrl embryos and n=4 cKO embryos from 2 litters. **b.** Total E9.5 yolk sac cells from Ctrl (*Drosha*<sup>fl/+</sup>; *Cdh5-cre*<sup>+</sup> or *Drosha*<sup>fl/fl</sup>, or *Drosha*<sup>fl/+</sup>) or cKO (*Drosha*<sup>fl/fl</sup>; *Cdh5-cre*<sup>+</sup>) mice were subjected to colony formation (CFU) assay. Colony counts are plotted as means ± SEM. n=5 Ctrl embryos and n=4 cKO embryos from 1 litter. **c.** Representative images of flow cytometry analysis on pro-erythroblasts (I:

CD71<sup>high</sup>Ter119<sup>low</sup>) and erythroblasts (II: CD71<sup>high</sup>Ter119<sup>high</sup>) derived from peripheral blood (PB) of E10.5 Ctrl or cKO embryos (upper panel). Mean fraction (%) of each population per total live (DAPI<sup>-</sup>) cells is indicated. n=8 Ctrl embryos and n=4 embryos from 2 litters. **d.** Representative images of flow cytometry analysis on erythroblasts at different stages from E13.5 fetal liver from Ctrl or cKO embryos (upper panel). Mean fraction (%) of each population per total live (DAPI<sup>-</sup>) cells is indicated. n=8 Ctrl embryos and n=4 cKO embryos from 3 litters. **e.** qRT-PCR analysis of different mRNAs (relative to GAPDH) in erythroid population of the PB of E10.5 Ctrl and cKO embryos is plotted as Mean  $\pm$  SEM. n=3 independent experiments with n=5 Ctrl embryos and n=5 cKO embryos from 3 litters. **f.** Gata1 protein amount was measured by immunoblot using CD71<sup>+</sup>Ter119<sup>+</sup> cells from E11.5 Ctrl and cKO PB or E12.5 Ctrl or cKO FL (left). Relative amount of Gata1 normalized to GAPDH was plotted as means  $\pm$  SEM (middle). For E11.5 PB, n=3 independent experiments with n=5 Ctrl embryos and n=8 cKO embryos from 3 litters. For E12.5 FL, n=3 independent experiments with n=7 Ctrl embryos and n=5 cKO embryos from 3 litters. *Gata1* mRNA was evaluated by qRT-PCR in total RNA prepared from E11.5 Ctrl or cKO PB or E12.5 Ctrl or cKO FL and plotted as means  $\pm$  SEM. For E11.5 PB, n=3 independent experiments with n=5 Ctrl embryos and n=5 cKO embryos from 3 litters. For E12.5 FL, n=3 independent experiments with n=6 Ctrl embryos and n=4 cKO embryos from 2 litters. **g.** K562 cells expressing CRISPR/Cas9 targeting *Drosha* (*Drosha* KO) or non-specific control (Ctrl) were treated with or without proteasome inhibitor MG132 (5 nM) for 6 hr prior to the preparation of total cell lysates, which were immunoblotted for Gata1 and GAPDH (as a loading control). n=3 independent experiments. **h.** Polysome fractionation of Ctrl or *Drosha* KO K562 cells. Top panels: Polysome profile of Ctrl or *Drosha* KO K562 cells. Bottom panel: qRT-PCR analysis of *Gata1* (black and red lines) and *ATF4* mRNAs (orange and blue lines) from each fraction normalized to 18S rRNA shown as means $\pm$ SEM; n=3 independent experiments with n=3 samples per genotype. Unpaired two-tail t-test was used for statistical analysis in all panels.



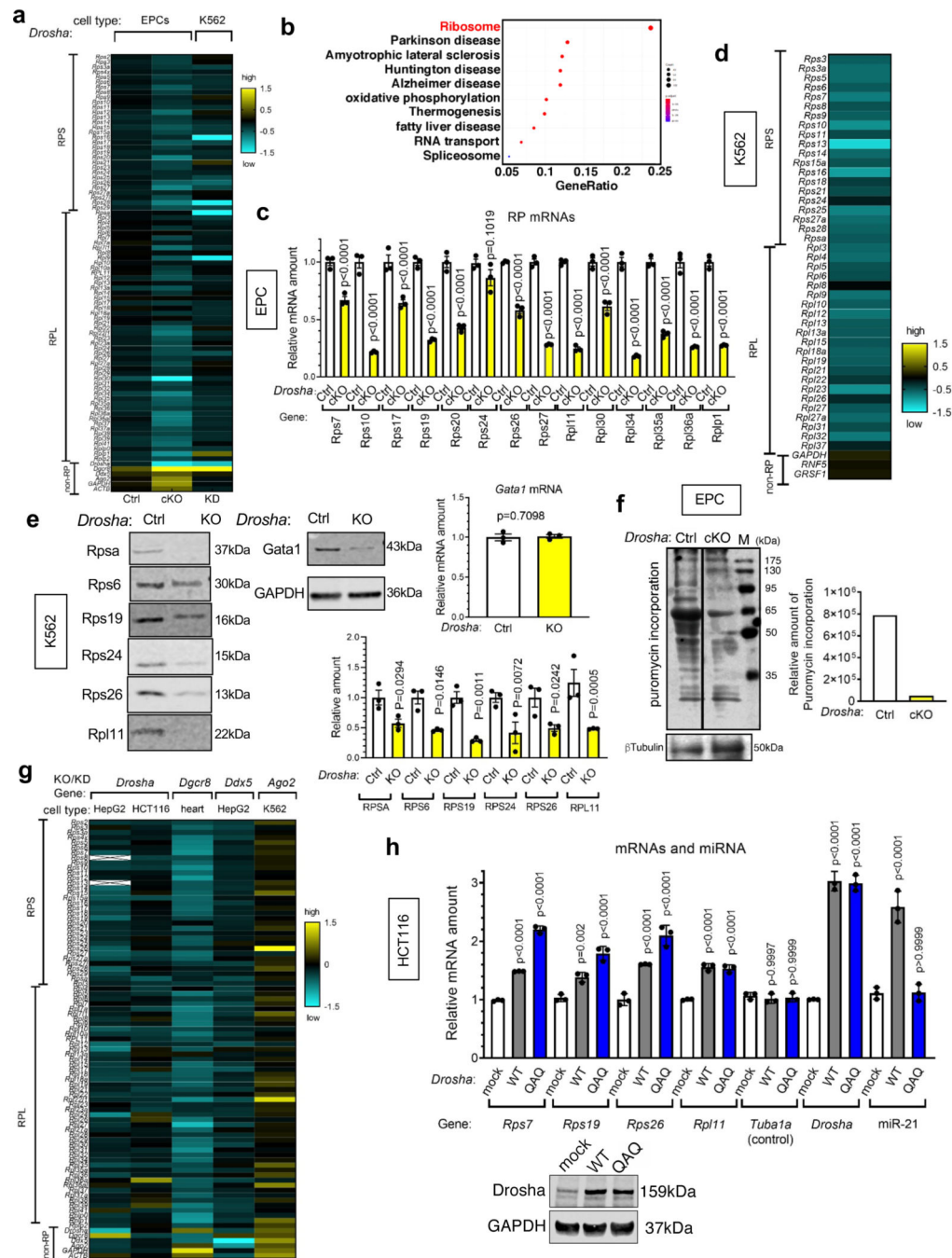


**Fig. 2. Reduced translation of Gata1 in *Drosha*-null erythroid progenitors.**

**a.** Heatmap of the changes in expression of mRNAs encoding RPs in EPCs ( $CD71^{high}Ter119^{+}$ ) sorted from E10.5 Ctrl and cKO PB.  $n=5$  Ctrl embryos and  $n=5$  cKO embryos from 3 litters. Heatmap of the changes in expression of mRNAs encoding RPs in *Drosha* KD K562 cells compared to Ctrl K562 cells is plotted in the right lane.  $\log_2$ (fold changes relative to ctrl) is plotted.  $n=3$  samples per genotype. **b.** KEGG pathway analysis of the transcriptomes of EPCs ( $CD71^{high}Ter119^{+}$ ) sorted from E10.5 Ctrl and cKO PB. **c.** qRT-PCR analysis of mRNAs (relative to GAPDH) in EPCs sorted from E10.5 Ctrl and cKO PB

is plotted as means  $\pm$  SEM. n=3 independent experiments with n=5 Ctrl embryos and n=5 cKO embryos from 3 litters. **d.** Equal numbers ( $3 \times 10^5$  cells) of Ctrl and Drosha KO K562 cells were subjected to TMT-based mass-spectrometric analysis. Log<sub>2</sub>(fold changes relative to ctrl) is plotted. The amounts of RPs or negative control proteins in KO compared to Ctrl cells are plotted as a heatmap. n=5 samples per genotype. **e.** Total cell lysates from Ctrl or *Drosha* KO K562 cells were immunoblotted for the indicated RPs in quadruplicate. Representative image of the immunoblots (left) and relative amounts of RPs normalized to GAPDH are plotted as means  $\pm$  SEM (bottom). n=4 independent experiments. *Gata1* mRNA was analyzed by qRT-PCR in Ctrl or Drosha KO K562 cells and plotted on the right as means  $\pm$  SEM (top, right). n= 3 independent experiments. **f.** Total cell lysates were generated from equal numbers ( $3 \times 10^5$  cells) of EPCs from the PB of E11.5 Ctrl and cKO embryos from puromycin-injected pregnant mice and were immunoblotted for puromycin and  $\beta$ -Tubulin (as a loading control) (left). The puromycin signal normalized to  $\beta$ -Tubulin was plotted (right). n=5 Ctrl embryos and n=5 cKO embryos from 3 litters. M, molecular weight marker. **g.** Heatmap of the changes in expression of mRNAs encoding RPs. The gene that is knocked down and the cell type are indicated over the heat map columns. Log<sub>2</sub>(fold changes relative to ctrl) is plotted. Crossed (X) cells: lack of data. n=2 samples per genotype for HepG2 Ctrl and Drosha KO cells. n=1 sample per genotype for HCT116 Ctrl and Drosha KO cells. n=76 single cardiomyocytes per genotype for Ctrl and Dgcr8 KO. n=3 samples per genotype for HepG2 Ctrl and Ddx5 KD cells. n=3 samples per genotype for K562 Ctrl and Ago2 KD cells. **h.** Human HCT116 cells were transfected with vector (mock), WT Drosha (WT) or the RNase-defective Drosha mutant (QAQ) construct. qRT-PCR analysis was performed *Rps/Rpl*-encoding mRNAs (relative to  $\beta$ -actin), *Tuba1a* (control), *Drosha* and miR-21 and are plotted as means  $\pm$  SEM. n= 3 independent experiments. Unpaired two-tail t-test was used for statistical analysis in all panels.

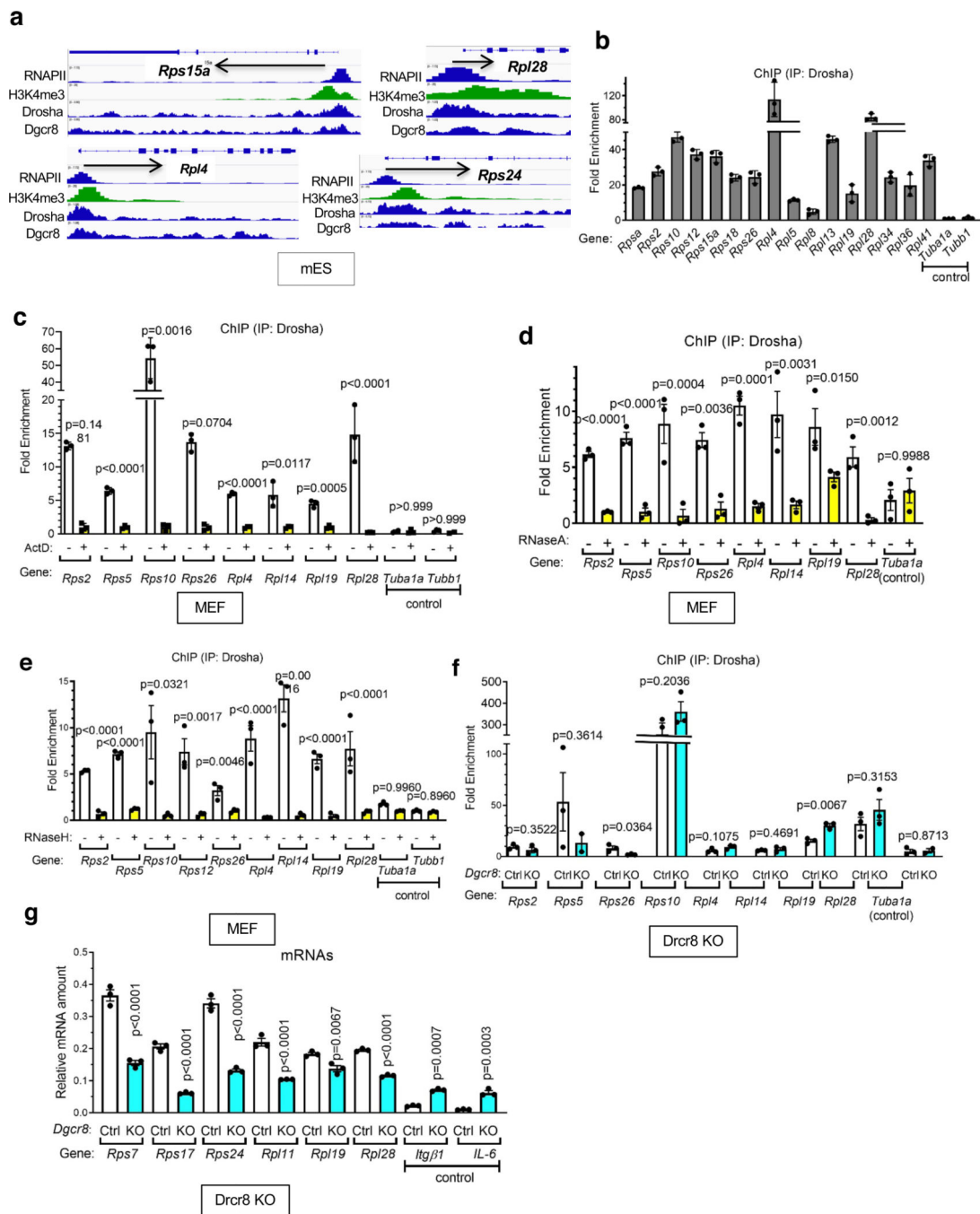


**Fig. 3. RPG transcripts are bound to the Microprocessor complex.**

**a.** ChIP-seq profiles of RNAPII(84), H3K4me3(84), Drosha and Dgcr8(53) at the *Rps15a*, *Rps24*, *Rpl4*, and *Rpl28* loci in mouse embryonic stem (mES) cells. **b.** ChIP-qPCR analysis of different RPGs in Flag (M2) antibody or nonspecific IgG (control) immunoprecipitates (IPs) from Flag-tagged Drosha-expressing MEFs or vector-expressing control MEFs. Fold enrichment of Flag IP over IgG IP is plotted as means  $\pm$  SEM. n=3 independent experiments. **c.** ChIP-qPCR analysis of different RPGs in Flag (M2) antibody or nonspecific IgG (negative control) IPs from Flag-Drosha-expressing MEFs or control MEFs treated with

Actinomycin D (ActD) or vehicle (DMSO). Fold enrichment of Flag IP over IgG IP is plotted as means  $\pm$  SEM. n=3 independent experiments. **d.** ChIP-qPCR analysis of different RPGs in Flag (M2) antibody or nonspecific IgG (negative control) IPs from MEFs treated with 1 $\mu$ g/ $\mu$ l RNase A or vehicle (water). Fold enrichment of Drossha IP over IgG IP is plotted as means  $\pm$  SEM. n=3 independent experiments. **e.** ChIP-qPCR analysis of different RPGs in Flag (M2) antibody or nonspecific IgG (negative control) IPs from MEFs treated with RNase H or vehicle (water). Fold enrichment of Drossha IP over IgG IP is plotted as means  $\pm$  SEM. n=3 independent experiments. **f.** ChIP-qPCR analysis of different RPGs in Flag (M2) antibody or nonspecific IgG (negative control) IPs from control MEFs (Ctrl) or MEFs lacking *Dgcr8* (Dgcr8-KO). Fold enrichment of Drossha IP over IgG IP is plotted as means  $\pm$  SEM. n=3 independent experiments. **g.** qRT-PCR analysis of different RP-encoding mRNAs and control mRNAs (relative to *GAPDH*) in Ctrl or Dgcr8-KO MEFs. Results are plotted as means  $\pm$  SEM. n=3 independent experiments.

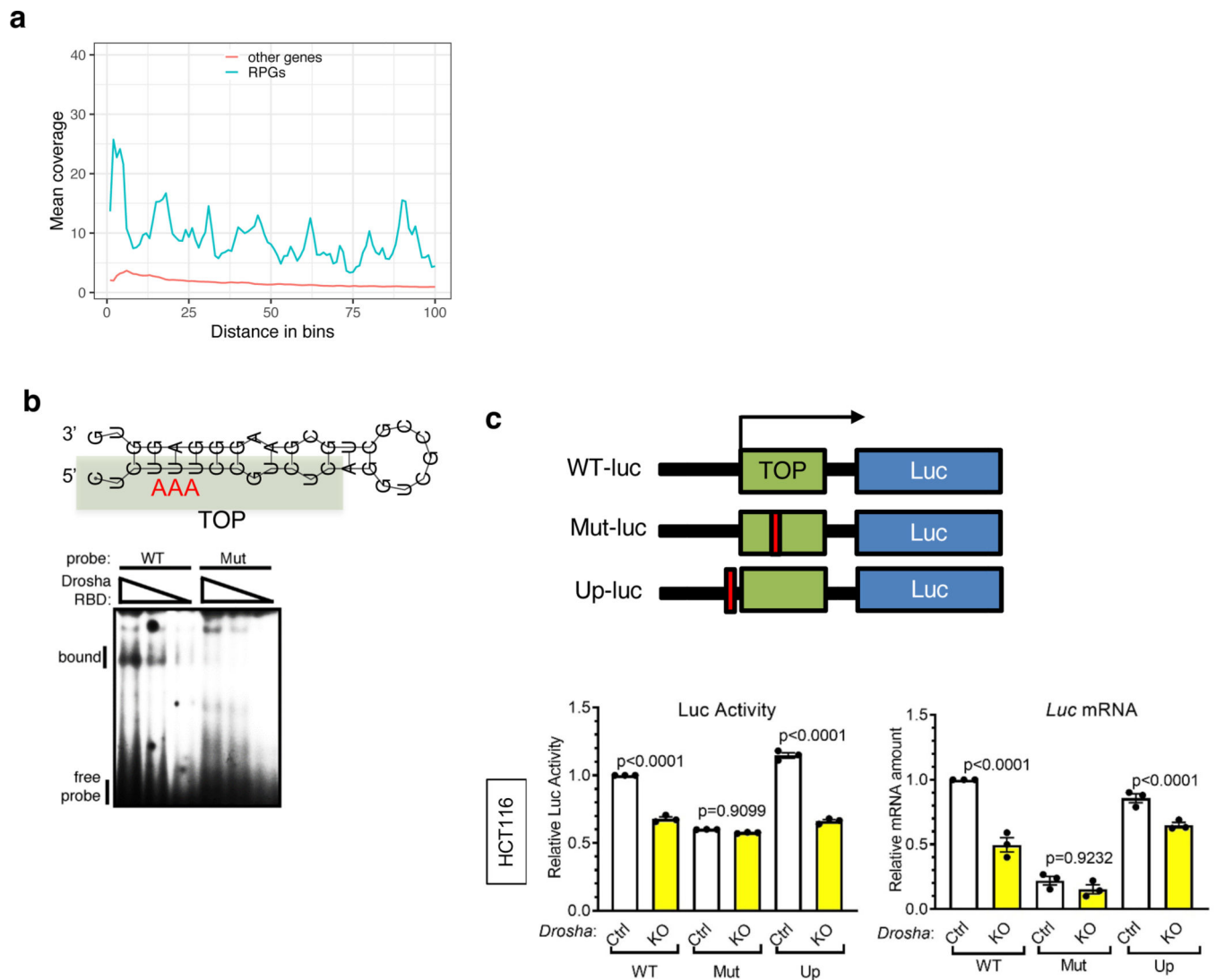


**Fig. 4. Association of the Microprocessor complex with the 5'-TOP motif.**

**a.** Metagene analysis of Drosha eCLIP(55) in K562 cells. Blue and red lines indicate average reads mapping to each position across RPGs or other non-RPG transcripts, respectively. X axis indicates the distance from the TSS (0). The bin size is 20-nt.  $n=2$  samples per genotype. **b.** The predicted structure of the WT probe and mutated nucleotides are shown. The TOP motif is indicated as a shaded box. Representative image of RNA EMSA with radiolabeled WT or Mut probe mixed with Drosha RBD.  $n=3$  independent experiments. **c.** The WT or mutant (Mut) *Rpl28* gene fragment (-38 to +11) was inserted upstream of the luciferase (Luc) gene. In the Up-Luc construct, the nucleotides upstream of the TSS were mutated. The green boxes indicate the TOP motif and the red boxes indicate the location of mutated sequence. Luciferase assays were performed in HCT116 cells expressing CRISPR/Cas9 targeting *Drosha* (*Drosha* KO) or a non-specific control (Ctrl) and the indicated luciferase reporter. Luciferase activity (left) and qRT-PCR analysis for luciferase reporter-encoding mRNAs (right) are plotted as means  $\pm$  SEM.  $n=3$  independent experiments. Unpaired two-tail t-test was used for statistical analysis in all panels

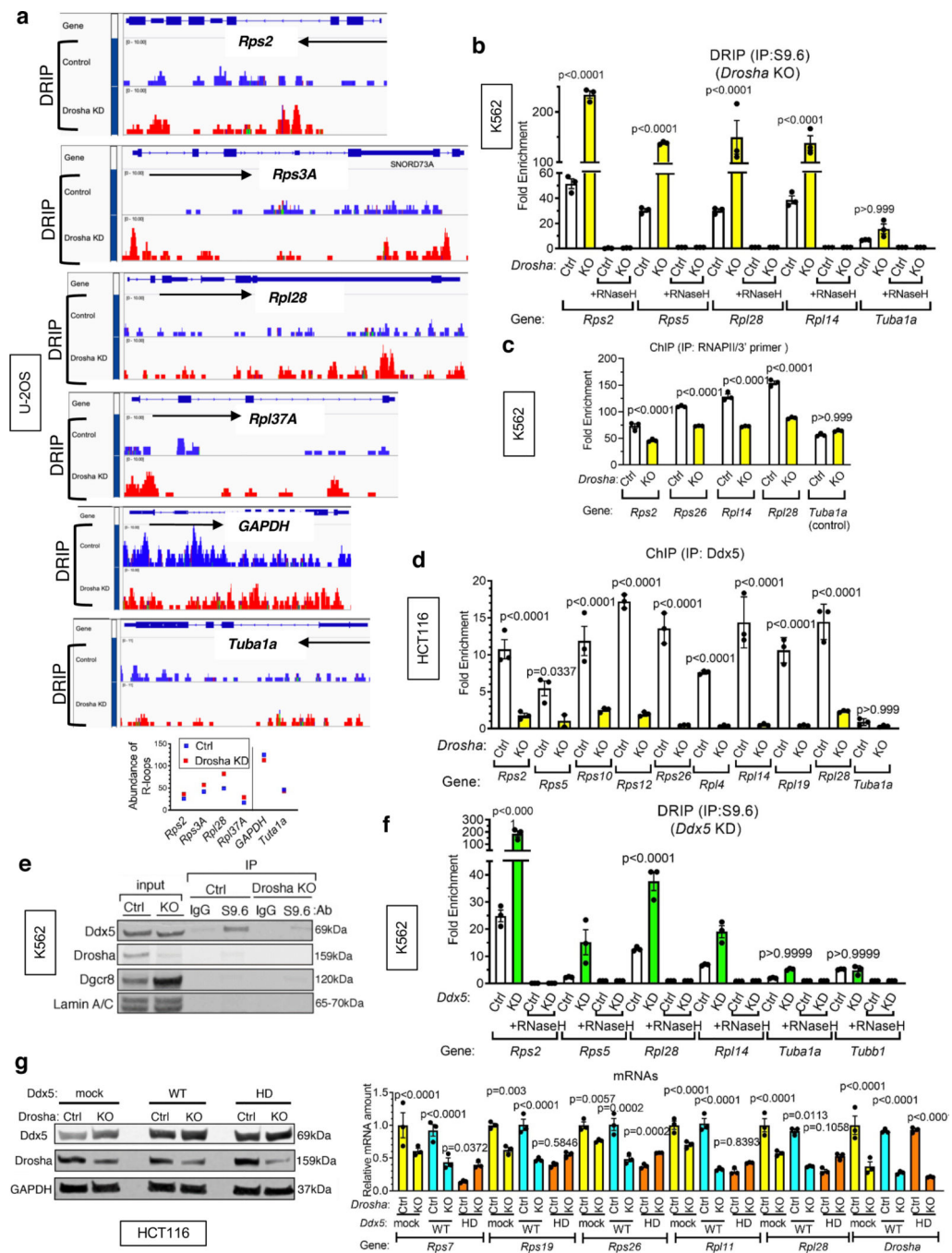


**Fig. 5. Ddx5 reduces DNA/RNA hybridization and facilitates transcription elongation.**  
**A.** DNA/RNA hybrid IP-sequencing (DRIP-seq) data for R-loop formation at RPG loci (*Rps2*, *Rps3A*, *Rpl28*, and *Rpl37A*) and control loci (*GAPDH* and *Tuba1a*) in Drosha KD cells (red) compared to control U2OS cells (blue) (top). Quantitation of the DRIP-seq data is shown (bottom). n=2 samples per genotype. **b.** DRIP analysis of RPG loci (*Rps2*, *Rps5*, *Rpl28*, and *Rpl14*) and a control locus (*Tuba1a*) in the presence or absence of RNase H in HCT116 cells expressing CRISPR/Cas9 against *Drosha* (KO) or non-specific control (Ctrl). Signals relative to input are plotted as means  $\pm$  SEM. n=3 independent experiments. **c.** ChIP-

qPCR analysis using RNAPII antibody and the 3' primer was performed in K562 cells expressing CRISPR/Cas9 against *Drosha* (KO) or non-specific control (Ctrl). Primers for RPG loci (*Rps2*, *Rps5*, *Rpl28*, and *Rpl14*) and a control locus (*Tuba1a*) are shown as means  $\pm$  SEM. n=3 independent experiments. **d.** ChIP-qPCR analysis using Ddx5 antibody of the indicated RPG and control loci in control (Ctrl) or *Drosha* KO HCT116 cells. Fold enrichment of Ddx5 antibody pull-down over IgG pull-down is plotted as means  $\pm$  SEM. n=3 independent experiments. **e.** Representative image of IPs with the S9.6 antibody to pull down DNA/RNA hybrids immunoblotted for Ddx5, Drosha, Dgcr8 and Lamin A/C (which was a negative control) in Ctrl or Drosha KO K562 cells. n=3 independent experiments. **f.** DRIP analysis of the indicated RPG and control loci in the presence or absence of RNase H in K562 cells with *Ddx5* RNAi (*Ddx5* KO) or non-specific control (Ctrl). Results are plotted as means  $\pm$  SEM. n=3 independent experiments. **g.** Drosha, Ddx5 and GAPDH proteins were examined by immunoblot in total HCT116 cell lysates (left). qRT-PCR analysis of the indicated mRNAs (relative to GAPDH) in Ctrl or *Drosha* KO HCT116 cells transfected with empty plasmid (mock), WT Ddx5 (WT) plasmid or the RNA helicase-defective (HD) mutant plasmid. Data are plotted as means  $\pm$  SEM (right). n=3 independent experiments. Unpaired two-tail t-test was used for the statistical analysis in all panels.

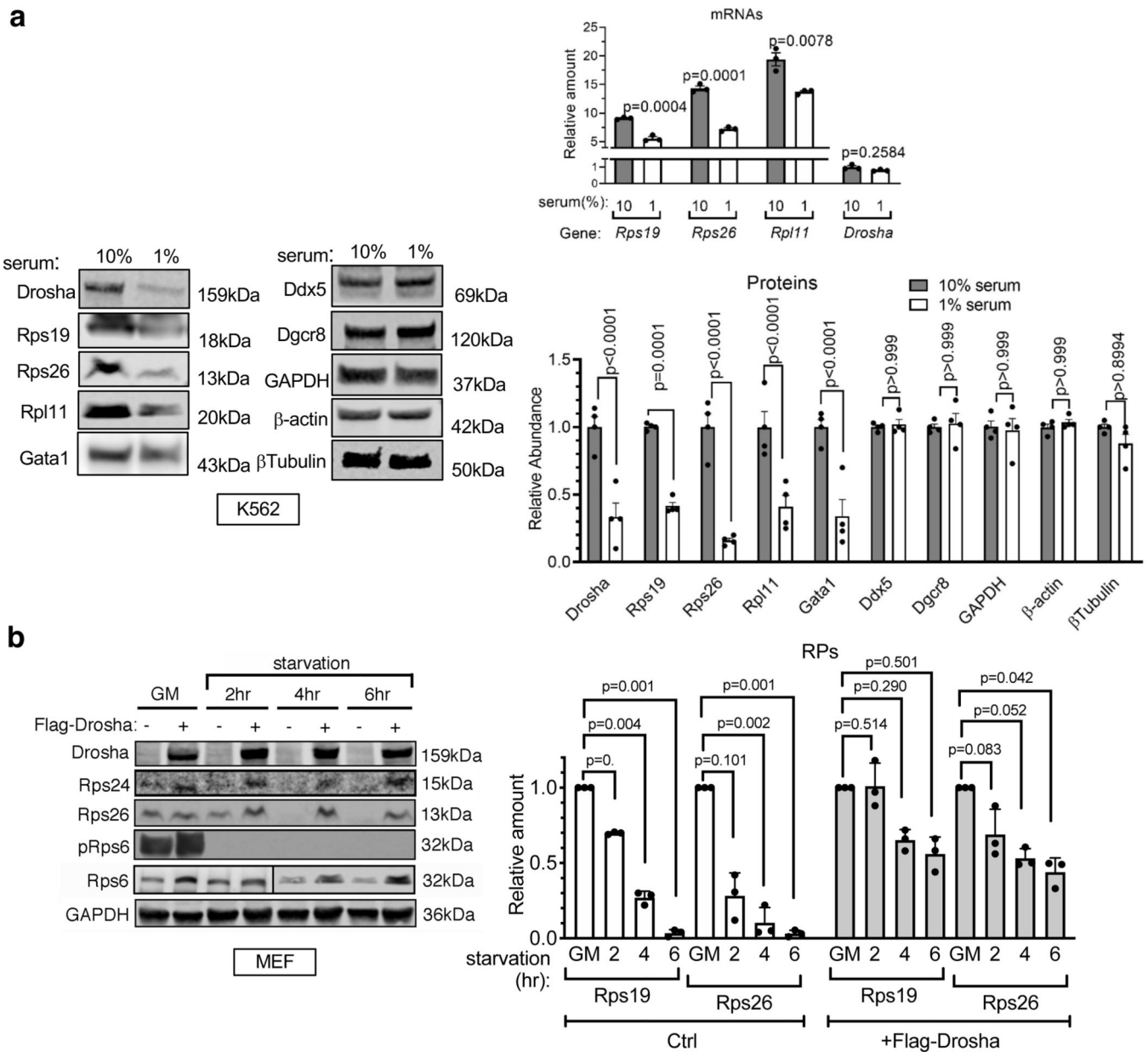


**Fig. 6. Nutrient starvation depletes Drosha and inhibits RP biosynthesis.**

**a.** K562 cells cultured in serum-starved (1% serum) or normal (10% serum) media for 6 hr (left) were immunoblotted for the indicated proteins in quadruplicate. Representative immunoblot image (left and middle) and relative protein amounts normalized to GAPDH are plotted as means  $\pm$ SEM (bottom right).  $n=4$  independent experiments. qRT-PCR analysis of the indicated mRNAs normalized to *GAPDH*. Data are plotted as means  $\pm$  SEM (right).  $n=3$  independent experiments. **b.** Drosha-expressing or Ctrl MEFs cultured in growth media (GM, 10% serum) or starvation media (no serum) for the indicated periods of time were immunoblotted for the indicated proteins in triplicate (left). The relative amounts of Rps24 and Rps26 normalized to GAPDH are plotted as means  $\pm$ SEM (right).  $n=3$  independent experiments. pRps6, phospho-Rps6.



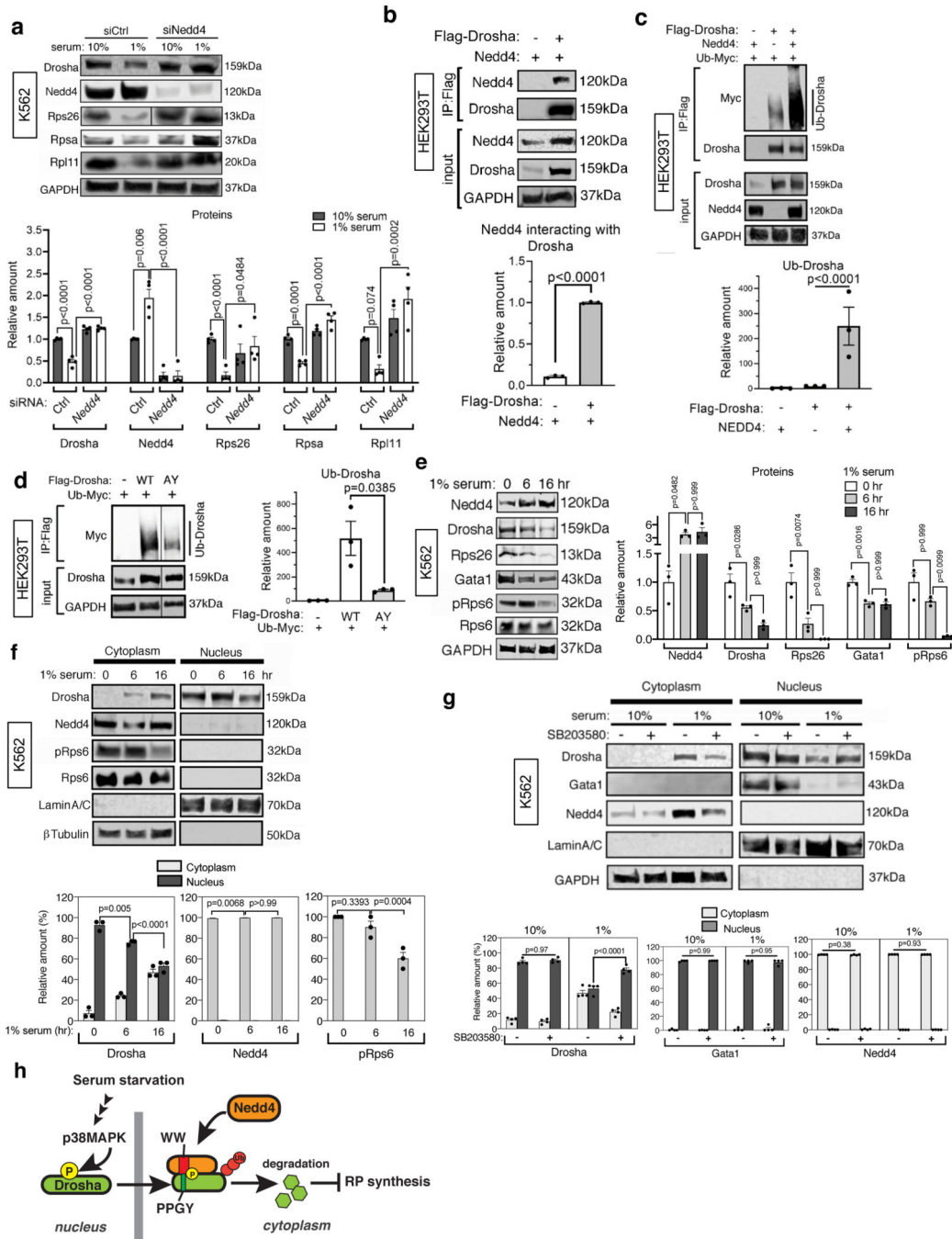


**Fig. 7. Degradation of Drosha by Nedd4 in the cytoplasm upon serum starvation.**

**a.** K562 cells transfected with non-specific control siRNA (siCtrl) or siRNA against Nedd4 (siNedd4) and cultured in growth media (10% serum) or serum starvation media (1% serum) for 6 hr were immunoblotted for the indicated proteins in quadruplicate. Relative protein amounts were normalized to GAPDH. Data are plotted as means  $\pm$ SEM (bottom). n=4 independent experiments. **b.** Association of Drosha with Nedd4 was examined in HEK293T cells expressing Flag-Drosha. Flag IPs were immunoblotted for Nedd4 and Flag (top) in triplicate. Total cell lysates (input) were immunoblotted for Nedd4, Drosha, and GAPDH

(loading control) (top). The relative amount of Nedd4 that precipitated with Flag-Drosha is plotted as means+SEM (bottom). n=3 independent experiments. **c.** Empty vector (pcDNA; mock) or Flag-tagged Drosha were expressed with Myc-tagged ubiquitin (Ub-Myc) in the presence or absence of Nedd4 in HEK293T cells. Flag IPs were immunoblotted for Myc to detect Ub-Drosha and Drosha in quadruplicate. Input samples were immunoblotted for Drosha and GAPDH (control). Representative image of the immunoblot (top) and relative amounts of Ub-Drosha normalized to Drosha (bottom) are plotted as means±SEM. n=4 independent experiments. **d.** Flag-tagged Drosha (WT or AY mutant) and Ub-Myc were exogenously expressed in HEK293T cells. Flag IPs were immunoblotted for Myc to detect Ub-Drosha in triplicate (left). Total cell lysates (input) were immunoblotted for Drosha and GAPDH (control). Relative amounts of Ub-Drosha normalized to Drosha are shown as means +SEM (right). n=3 independent experiments. **e.** K562 cells under serum starvation (1% serum) for 0, 6 or 16 hr were immunoblotted for the indicated proteins in quadruplicate. Representative image of the immunoblot (left) and relative protein amounts normalized to GAPDH are shown as means ±SEM (right). n=4 independent experiments. **f.** Cytoplasmic and the nuclear fractions were prepared from K562 cells that were serum starved (1% serum) for 0, 6, or 16 hr. Fractions were immunoblotted for Drosha, Nedd4, phospho-Rps6 (pRps6, control for cytoplasmic fraction), Rps6, Lamin A/C, and βTubulin in quadruplicate (top). Relative amounts of Drosha and Nedd4 normalized to βTubulin (for cytoplasmic fraction) or Lamin A/C (for nuclear fraction) and pRps6 normalized to Rps6 in the cytoplasm and nucleus (%) are quantitated and shown as means±SEM (bottom). n=4 independent experiments. **g.** Cytoplasmic and the nuclear fractions were prepared from K562 cells were cultured in 10% or 1% serum containing media with vehicle (DMSO) or SB203580 (10 mM) for 16 hr. Fractions were immunoblotted for Drosha, Gata1, Nedd4, Lamin A/C (control for nuclear fractions) and GAPDH (control for cytoplasmic fractions) in quadruplicate (top). Relative amount of Drosha, Gata1, or Nedd4 normalized to GAPDH (for cytoplasmic fractions) or Lamin A/C (for nuclear fraction) in the cytoplasm and nucleus (%) are shown as means±SEM (bottom). n=4 independent experiments. One-way ANOVA followed by Tukey's multiple comparisons test was used in **e** and **f**. Unpaired two-tail t-test was used in the other panels. **h.** Schematic diagram of Nedd4-dependent regulation of Drosha. Serum starvation promotes the phosphorylation of Drosha by p38 MAPK in the nucleus, which induces the nuclear export of Drosha. In the cytoplasm, the WW domain of Nedd4 associates with the PPGY motif of Drosha, resulting in the ubiquitination and degradation of Drosha. As a result, RP biosynthesis is inhibited.

**Table 1:**

Association of Drosha and Dgcr8 with Rps and Rpl-encoding transcription start sites (TSS) by ChIP-seq.

	<b>RPS</b>	<b>Binding Site</b>	<b>RPL</b>	<b>Binding Site</b>
Drosha	<i>Rps2</i>	TSS(+44)	<i>Rpl3</i>	TSS
	<i>Rps3</i>	TSS	<i>Rpl4</i>	TSS(+25)
	<i>Rps4</i>	Intron(+250–450)	<i>Rpl5</i>	TSS(–47)
	<i>Rps5</i>	-650	<i>Rpl6</i>	TSS(+83)
	<i>Rps6</i>	intron	<i>Rpl7</i>	TSS(+59)
	<i>Rps7</i>	1 <sup>st</sup> intron	<i>Rpl8</i>	TSS(+35)
	<i>Rps8</i>	1 <sup>st</sup> intron	<i>Rpl10</i>	TSS(–720)
	<i>Rps9</i>	TSS	<i>Rpl12</i>	TSS(–35)
	<i>Rps10</i>	TSS(–236)	<i>Rpl13</i>	TSS(–29)
	<i>Rps11</i>	TSS(–450)	<i>Rpl13a</i>	TSS(37)
	<i>Rps12</i>	TSS(+55)	<i>Rpl14</i>	Intron(391)
	<i>Rps13</i>	TSS	<i>Rpl15</i>	TSS(–21)
	<i>Rps15a</i>	TSS(+41)	<i>Rpl17</i>	TSS(–239)
	<i>Rps17</i>	TSS(–80)	<i>Rpl18</i>	TSS(+866)
	<i>Rps18</i>	TSS(–46)	<i>Rpl19</i>	TSS(+53)
	<i>Rps19</i>	TSS(–10)	<i>Rpl22</i>	TSS(+85)
	<i>Rps20</i>	TSS	<i>Rpl2211</i>	TSS(+24)
	<i>Rps23</i>	1 <sup>st</sup> intron(+220)	<i>Rpl27a</i>	TSS(+27)
	<i>Rps24</i>	TSS(+10)	<i>Rpl28</i>	TSS(–272)
	<i>Rps25</i>	TSS?	<i>Rpl32</i>	TSS(–49)
	<i>Rps26</i>	TSS(+21)	<i>Rpl34</i>	TSS(–217)
	<i>Rps27</i>	exon(+120)	<i>Rpl35</i>	Intron (611)
	<i>Rps27a</i>	TSS(–234)	<i>Rpl36</i>	TSS(+51)
	<i>Rps28</i>	TSS(+25)	<i>Rpl37a</i>	TSS(+56)
	<i>Rps29</i>	TSS(–80)	<i>Rpl41</i>	TSS(+569)
<i>Rpsa</i>	TSS(+35)	<i>Rplp0</i>	TSS(+26)	
Dgcr8	<i>Rps9</i>	Intron(+534)	<i>Rpl3</i>	TSS(+165)
	<i>Rps11</i>	TSS(–993)	<i>Rpl5</i>	Intron(+686)
	<i>Rps12</i>	TSS(+665)	<i>Rpl7a</i>	TSS(+44)
	<i>Rps15</i>	Intron(+495)	<i>Rpl711</i>	TSS(+66)
	<i>Rps18</i>	TSS(–40))	<i>Rpl8</i>	TSS(+60)
	<i>Rps24</i>	Intron(+1889)	<i>Rpl10a</i>	TSS(+96)
	<i>Rpsa</i>	Intron(+513)	<i>Rpl11</i>	Intron(+436)
			<i>Rpl12</i>	TSS(–30)
			<i>Rpl13a</i>	TSS(+8)
			<i>Rpl2211</i>	TSS(+44)

<b>RPS</b>	<b>Binding Site</b>	<b>RPL</b>	<b>Binding Site</b>
		<i>Rpl24</i>	TSS(+7)
		<i>Rpl26</i>	TSS(-63)
		<i>Rpl28</i>	Intron(+694)
		<i>Rpl30</i>	TSS(-16)
		<i>Rpl34</i>	TSS(-191)
		<i>Rpl37a</i>	TSS(+50)
		<i>Rpl41</i>	TSS(+153)
		<i>Rpl1</i>	TSS(+403)

Author Manuscript

Author Manuscript

Author Manuscript

Author Manuscript